Sci. Dril., 35, 99–117, 2026
https://doi.org/10.5194/sd-35-99-2026

Scientific Drilling
Open Access

The ICDP Nam Co Drilling Project (NamCore), Tibet: a 510.2 m sedimentary record from the Third Pole

Marie-Luise Adolph[1], Junbo Wang[2], Liping Zhu[2], Leon J. Clarke[3], Andrew C. G. Henderson[4], Hendrik Vogel[5], Gerhard Daut[6], Peter Frenzel[7], Jianting Ju[2], Qiangqiang Kou[2], Dierk Michaelis[8], Olga Schmitz[7], Anja Schwarz[9], Volkhard Spiess[10], Arne Ulfers[11], Cidan Zhaxi[2], Daniel Ariztegui[12], Natasha Barbolini[13], Thorsten Bauersachs[14], Erwin Braun[1], Giulia Ceriotti[15], Brian Grivna[16], Marlene Hoehle[17], Rolf Kipfer[18], Wilhelmine Klamt[1], Cindy Kunkel[19], Aliisa Laakkonen[5], Minghui Li[2], Qingfeng Ma[2], Paul Moser Röggla[18], Kaja Müller[1], Anders Noren[16], Ryan O'Grady[16], Santiago Otero[1], Maïlys Picard[5], Anna Pint[7], Camille Thomas[5], Jerome Van der Woerd[20], Mathias Vinnepand[11], Claudia Wrozyna[17], Christian Zeeden[11], Xinghuan Zhu[2], and Torsten Haberzettl[1]

[1]Physical Geography, Institute for Geography and Geology, University of Greifswald, Greifswald, Germany
[2]Institute of Tibetan Plateau Research, Chinese Academy of Sciences, China, Beijing, China
[3]Department of Natural Sciences, Faculty of Science and Engineering, Manchester Metropolitan University, Manchester, UK
[4]School of Geography, Politics & Sociology, Newcastle University, Newcastle upon Tyne, UK
[5]Institute of Geological Sciences & Oeschger Centre for Climate Change Research, University of Bern, Bern, Switzerland
[6]Physical Geography, Institute of Geography, Friedrich Schiller University Jena, Jena, Germany
[7]General and Historical Geology, Institute of Geosciences, Friedrich Schiller University Jena, Jena, Germany
[8]Institute of Botany and Landscape Ecology, University of Greifswald, Greifswald, Germany
[9]Institute of Geosystems and Bioindication, Technische Universität Braunschweig, Braunschweig, Germany
[10]Department of Geosciences, University of Bremen, Bremen, Germany
[11]Petrophysical Characterization, LIAG-Institute for Applied Geophysics, Hannover, Germany
[12]Department of Earth Sciences, University of Geneva, Geneva, Switzerland
[13]Department of Ecology, Environment and Plant Sciences and Bolin Centre for Climate Research, Stockholm University, Stockholm, Sweden
[14]Institute of Organic Biogeochemistry in Geo-Systems, RWTH Aachen University, Aachen, Germany
[15]Institute of Earth Surface Dynamics, University of Lausanne, Lausanne, Switzerland
[16]Continental Scientific Drilling Facility, University of Minnesota, Minneapolis, USA
[17]Paleontology, Institute for Geography and Geology, University of Greifswald, Greifswald, Germany
[18]Department of Water Resources and Drinking Water, Eawag, Swiss Federal Institute of Aquatic Science and Technology, Duebendorf, Switzerland
[19]Geomechanics and Scientific Drilling, GFZ Helmholtz Centre for Geosciences, Potsdam, Germany
[20]Institut Terre et Environnement de Strasbourg, CNRS, University of Strasbourg, Strasbourg, France

Correspondence: Marie-Luise Adolph (marie-luise.adolph@uni-greifswald.de), Junbo Wang (wangjb@itpcas.ac.cn), Liping Zhu (lpzhu@itpcas.ac.cn), and Torsten Haberzettl (torsten.haberzettl@uni-greifswald.de)

Received: 26 January 2026 – Revised: 21 April 2026 – Accepted: 29 April 2026 – Published: 5 June 2026

Abstract. The Nam Co Drilling Project (NamCore) is a multinational and interdisciplinary research initiative designed to understand long-term climatic variability and associated environmental change on the Tibetan Plateau. The project primarily targets the timing and magnitude of Indian/East Asian monsoon variability and its interplay with the Westerlies. Thereby, the glacial–interglacial history and dynamics at high altitude; the impact of geological and environmental changes on (micro-)biological processes; the evolution and resilience of

high-altitude ecosystems, including the deep biosphere; and geomagnetic variations during the Quaternary are of special interest.

For in-depth investigations regarding the outlined research purposes, the (mostly) calcareous sediments of Nam Co, one of the largest and deepest lakes on the Tibetan Plateau, were targeted within the framework of the International Continental Scientific Drilling Program (ICDP) and cored in May–July 2024 (ICDP Expedition 5073). Altogether, 1415.45 m was drilled and 1175.99 m cored, with 950.77 m of sediment recovered (core recovery of 80.8 %) from seven holes at one site (5073_1) situated at a water depth of ∼ 93 m, reaching a maximum depth of 510.2 m below the lake floor. Initial results from core descriptions and preliminary core catcher analyses suggest that the sediments of Nam Co reflect the evolution of a dynamic high-altitude lake system over multiple glacial–interglacial cycles. Four major lithologies are observed in the drill cores (calcareous mud, non-calcareous mud, calcareous mud with ferric staining and sand) and grouped into five major lithological units based on their physicochemical characteristics obtained from core catcher material. Micropaleontological results from core catcher material reveal a general absence of diatoms, due to unsuitable growing and/or preservation conditions, while ostracods abundances, preservation, and species composition vary, which might be linked to environmental changes and/or changing preservation conditions. Shifts in *n*-alkane chain length might be attributable to lake-level variations and/or glacial–interglacial cycles.

1 Introduction and scientific objectives

The Tibetan Plateau, with its surrounding mountain ranges of the Hindu Kush, Karakoram, and Himalayas, is considered to be the Third Pole because its high-alpine ice fields store the largest volume of ice outside of the polar regions (United Nations Environment Programme, 2022). These ice reservoirs and large alpine lakes contribute to the idea of the Tibetan Plateau acting as an "Asian Water Tower" that feeds major Asian river systems, e.g. the Brahmaputra, Mekong, Yangtze, Yellow, Indus, and Ganges rivers. These river systems supply freshwater to almost two billion people downstream (Yao et al., 2022). This freshwater supply is closely linked to the hydroclimate changes of the Asian Water Tower, which is mainly modulated by large-scale atmospheric circulation systems, such as the Indian and East Asian Monsoons and the Westerly Jet circulation (Fig. 1). The interplay between the Indian Summer Monsoon and the Westerlies affects the spatial and temporal distribution of precipitation across the Tibetan Plateau and Southeast Asia (Kasper et al., 2015, 2021; Yao et al., 2013). However, the underlying forcing of longer-term monsoon variability remains under debate because of the variable influence of precession (e.g. speleothem and loess records; Guo et al., 2022) and eccentricity and obliquity (e.g. marine records; Clemens et al., 2016) on insolation-induced land–sea temperature contrasts. Tibetan Plateau climate is additionally affected by the impacts of climate boundary conditions, e.g. ice sheet volume and extent, greenhouse gas concentration, vegetation structure and coverage, changes in Atlantic Meridional Overturning Circulation (AMOC), on atmospheric circulation patterns and moisture transport (Chen et al., 2021; Stevens et al., 2018). In order to improve future climate change predictions, it is essential to understand the timing, duration, and intensity of past climatic variability in this sensitive high-altitude setting, where records covering long geological timescales are scarce. The isolated high-altitude setting of the Tibetan Plateau, a result of tectonic uplift that started 65–60 Myr ago (Ding et al., 2022), has led to unique terrestrial, aquatic, and subsurface ecosystems that are characterized by a large number of endemic species (e.g. von Oheimb et al., 2011). The Tibetan Plateau acted as both a source (centre of origin) and a sink (centre of accumulation) for numerous species, with a high net diversification between 2 Ma and 150 ka (Mosbrugger et al., 2018). Understanding the tectonic and climatic controls on the Tibetan Plateau and their link to species and functional diversity, as well as the evolution of these high-altitude, isolated ecosystems, will help unravel factors controlling the resilience of life in extreme environments, including over past glacial–interglacial cycles. In particular, long lake sediment records offer the unique opportunity to target sub-surface biodiversity in high-altitude, deeply buried sediments, an extreme environmental setting that has not been studied before in large-scale drilling projects (Ariztegui et al., 2015). The activity and diversity of the sub-surface biosphere are likely to be shaped by reciprocal interactions with climate-driven changes in carbon cycling, nutrient availability, redox conditions, and salinity variations. Understanding sub-surface microbial activity is thus essential as these feedbacks impact sediment composition through dissolution, alteration, and precipitation of minerals (Ariztegui et al., 2015).

To address these issues, the ICDP Nam Co Drilling Project (NamCore) targeted Nam Co ("Co" means lake in Tibetan) as one of the best-investigated, largest, and deepest lakes on the Tibetan Plateau. Nam Co was identified as a promising sediment archive that could yield one of the longest and most continuous sedimentary records from the high-altitude region, likely spanning the last 1 million years of Earth's history (Haberzettl et al., 2019). The Quaternary sedimentary

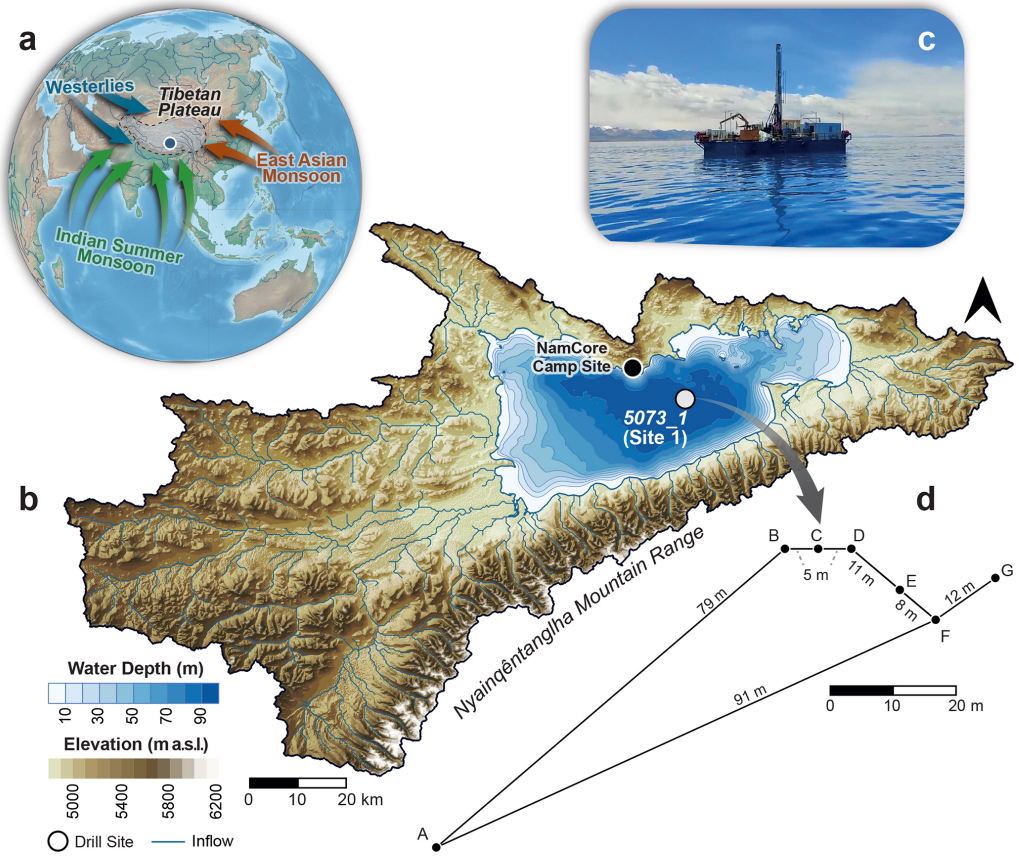

Figure 1. **(a)** Location of Nam Co on the Tibetan Plateau, including major atmospheric circulation systems. **(b)** Catchment and bathymetry of Nam Co, including major inflows (blue lines). The drill site 5073_1 (white dot) was located in the central part of Nam Co. To shorten transfer time to the drill site, a camp was constructed on the northern shoreline. **(c)** Barge on Nam Co. **(d)** The distance between the individual holes. Note that hole A has a larger distance to the other holes due to anchoring issues.

record in Nam Co provides the basis for addressing the following key scientific objectives:

i. long-term climate variability on the Tibetan Plateau and its relation to hemispheric and global atmospheric circulation patterns, including the timing and magnitude of Indian Summer Monsoon variability and its interplay with the Westerlies;

ii. the influence of orbital parameters, i.e. precession, eccentricity, or obliquity, on the Quaternary climate on the Tibetan Plateau;

iii. glacial history and dynamics on the Tibetan Plateau using a comparison of sediment core to seismic data and lake sediment proxies that reflect glacier growth and decay over glacial–interglacial timescales;

iv. impact of geological and environmental changes on (micro-)biological processes and evolution and resilience of high-altitude ecosystems under glacial–interglacial climate variations;

v. sub-surface deep biosphere at high altitudes, assessed qualitatively or quantitatively through the study of microbial-community diversity and rates of elemental cycling, including how microbial communities exploit tectonically formed habitats such as geogenic or fault-derived fluids and solutes to fuel their metabolism;

vi. geomagnetic changes and Earth's paleomagnetic field before the Holocene, capturing rates of change and the dynamic features of secular variation, as well as testing the importance of the Siberian flux lobe in relation to reconstructions of the global dipole moment;

vii. tectonic history and evolution of faulting to explore the timing of basin deformation and to validate models of source-to-sink geomorphology.

The sub-surface biosphere and how it may transform the sediments was addressed in Thomas et al. (2024). Moreover, we initially reported on the successful drilling campaign in Henderson et al. (2024), while the extensive drilling preparations, the drilling campaign, the core opening, and the sam-

pling parties were reported in detail in the operational report (Adolph et al., 2025). Therefore, in this contribution, we will only give a short overview of the drilling campaign, core opening, and sampling parties. We will show initial results, including the lithostratigraphic framework, which has been obtained from sediment core inspection and was corroborated by sedimentological, geochemical, and micropaleontological multi-proxy analyses on core catcher material. Additionally, we will provide a scientific outlook on the project.

2 Study site

Nam Co is a high-altitude lake (4718 m a.s.l.) situated in the central part of the Tibetan Plateau (90.690444° N, 30.746639° E, Fig. 1). The basin has a complex tectonic history and is located in the Paleozoic–Mesozoic "Lhasa block", between the Yarlung and Bangong sutures to the south and north (Pullen et al., 2008). The collision of the Indian Plate with the Eurasian Tectonic Plate has driven the uplift of the Tibetan Plateau since the Eocene (e.g. Aitchison et al., 2007; Gibbons et al., 2015). Although the timing and pace of construction of the continental Tibetan Plateau over the last 50 Myr remain debated (e.g. Ai et al., 2019; Ding et al., 2014; Xu et al., 2018), geological evidence suggests that Nam Co has been close to its present elevation since the late Miocene (12–10 Ma; Kapp et al., 2005). During the collision, the Gangdese volcanic arc, to which the Nyainqêntanglha Mountains belong (S and SW of Nam Co; Fig. 1), was exhumed. This mountain range was formed during the Cretaceous as a result of an Andean-type subduction (Ding et al., 2014). Subsequent uplift associated with normal faulting along the Gulu–Yanbaijin graben (Armijo et al., 1986) isolated the Nam Co catchment from the Yarlung–Brahmaputra drainage system. At present, the Nam Co catchment is one of the largest endorheic basins of the Tibetan Plateau (Wang et al., 2022).

The Nam Co basin is surrounded by several active faults, such as the Beng Co right-lateral strike–slip fault to the north, the left-lateral transtensional Damxung–Yanbajin fault system to the southeast, and normal faults in the Gulu graben to the east (Armijo et al., 1989; Chevalier et al., 2020; Taylor and Yin, 2009). These faults are responsible for some major regional earthquakes (M_w 7–8) across the past century, e.g. the 1951 Beng Co earthquake (M_w 7.7) and the 1952 (M_w 7.4) and 2008 (M_w 6.3) Damxung earthquakes (e.g. Armijo et al., 1989; Li et al., 2022; Wu et al., 2011).

The bathymetry of modern Nam Co is characterized by two sub-basins: a larger, central basin with a maximum water depth of ca. 99 m, on which the drilling activities were focused, and a smaller, shallower basin with a water depth of about 60 m in the northeast (Wang et al., 2009; Fig. 1). Nam Co covered an area of 2017 km^2 in 2022 (Zhu et al., 2025), while the catchment area comprised a total of 10 680 km^2 (Zhou et al., 2013). The drainage area includes more than 60 creeks, most of them originating from the Nyainqêntanglha Mountains in the south (> 7000 m a.s.l., Fig. 1; Wang et al., 2009). Modern Nam Co is an endorheic, dimictic, oligotrophic, slightly alkaline, and saline lake with stable thermal stratification during summer months (Wang et al., 2020).

The present climate of the Nam Co region is semi-arid to sub-humid with a mean annual air temperature of approximately 0 °C. The lake experiences an average ice cover duration of 90 d and is typically completely frozen from early February to mid-May (Wang et al., 2019). The mean annual wind speed is 4 m s^{-1}, with prevailing wind directions from southeast to west (Wang et al., 2019). Annual precipitation averages around 420 mm (Anslan et al., 2020; Wang et al., 2019). More than 90 % occurs as intense rainfall during the monsoon season between June and September (Maussion et al., 2014), while the period from October to May is exceptionally dry. As Nam Co is located in a closed basin, the lake water balance is primarily governed by precipitation and evaporation, with additional contributions from permafrost thaw, glacial meltwater, and groundwater inflow. The strong seasonality at Nam Co causes intra-annual lake level fluctuations of up to ∼ 0.8 m, which, in combination with a lake level increase of 2.2 m between 1980 and 2010 (Zhu et al., 2025), highlights the sensitivity of Nam Co to precipitation and evaporation dynamics. This assessment is further supported by fossil elevated lake terraces and also submerged beach ridges (Daut et al., 2010; Wrozyna et al., 2012).

3 Drilling strategy and core site selection

Site selection was based on four joint Sino-German hydroacoustic surveys carried out in 2005–2006, 2014, and 2016 and recording ∼ 1500 km of seismic profiles (Schulze, 2020). This extensive grid of sediment echo sounder and multichannel seismic profiles helped to develop a detailed understanding of the tectonic framework and sediment architecture of Nam Co. The seismic profiles show acoustically well-stratified reflections, indicating several hundred metres of sediment infill with varying thicknesses and steep faults with a spacings of several hundred metres, indicating a strike–slip tectonic regime (Fig. 2). These hydro acoustic surveys and their results are described in detail in Schulze (2020) and Haberzettl et al. (2019).

The drill site selection and coring strategy initially aimed to build a composite sedimentary record of three overlapping ∼ 150 m long sediment records from three drill sites along a NW–SE transect using an offset drilling approach with drilling sites at least 200 m away from faults (for details, see Haberzettl et al., 2019). Despite the relatively close occurrence (50 km) of a large magnitude-8 earthquake in relation to the drill sites, no evidence of large sediment perturbation has been observed that would impact the climatic record. Generally, the drilling approach would have enabled the recovery of a complete stratigraphy with maximum tem-

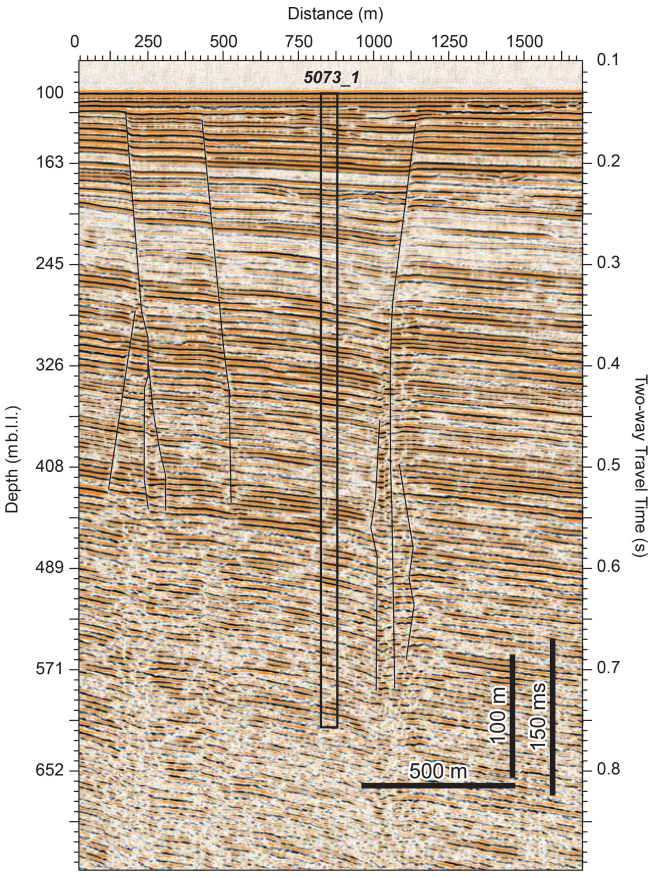

Figure 2. Multi-channel seismic profile ($V_p = 1630\,m\,s^{-1}$) at the NamCore 5073_1 coring site (see Fig. 1) showing several hundred metres of sediment infill and a sufficient distance to faults. The depth scale refers to metres below lake level (~ 90 m).

poral resolution while minimizing drilling depths, costs, and logistical challenges. Originally, these three sites should have been complemented by two additional sites (Haberzettl et al., 2019), but because drilling operations were limited to one field season, the drilling strategy was modified to reduce drilling time, pushing both additional sites to lower priorities (Adolph et al., 2025).

Based on pre-site surveys (e.g. Dietze et al., 2014; Doberschütz et al., 2013; Kasper et al., 2012, 2015), predominantly fine-grained sediments were expected given the water depth of ~ 93 m and a drilling location in the centre of the lake (Fig. 1). However, the recovered sediment sequence was intercalated by up to meter-thick unconsolidated medium to coarse sand deposits, which (i) frequently collapsed into the borehole, (ii) required large volumes of bentonite and polymer conditioned drilling fluids for stability, and (iii) required continuous use of rotary-drilling coring tools.

As a consequence, the coring operations team revisited the seismic stratigraphy and opted not to drill the two additional shallower-depth sites on the NW–SE transect as seismic data indicated the presence of potentially more extensive coarse-grained strata at these near-shore sites (Adolph et al., 2025; Haberzettl et al., 2019). Drilling at these sites would have likely resulted in even more challenging drilling operations with limited depth advance and reduced core recovery. Therefore, the operational decision was taken to focus solely on site 1 (5073_1, Fig. 1), which promised a recovery of a continuous sediment record of at least 300–450 m b.l.f. (metres below the lake floor) (Fig. 2, Adolph et al., 2025).

4 Drilling, logging, and scientific on-site operations

Drilling at high altitudes in rural Tibet required extensive preparations and planning. Following months of online meetings, major operational planning was advanced during and after site visits in China in June and September 2023 with the drilling contractor and manufacturers for the platform and work boat. After these meetings, further communications with manufacturers for the drill pipes, the camp contractor, and other service providers further developed the operational plan (Adolph et al., 2025). The soft sediment coring tools, used in numerous previous ICDP lake drilling projects, were purchased from QD Tech, Inc., and were shipped from the United States. Downhole logging probes were shipped from the Institute of Applied Geophysics (LIAG), Hanover, Germany, and a downhole logging winch from the ICDP Operational Support Group, GFZ Helmholtz Centre for Geosciences, Potsdam, Germany. A campsite and a simple wharf were constructed on the remote northern shore of Nam Co, thus reducing boat transportation time between camp and the barge at the drill site significantly (Fig. 1).

Drilling commenced on 6 June, with the first core on deck on 7 June, and concluded on 17 July 2024. The drill rig and associated equipment and drilling personnel were contracted through Sichuan Huafeng Drilling Co., Ltd., Chengdu, China. The Hydraulic Piston Corer (HPC) used in 5073_1_A and 5073_1_B was only suitable for the upper ~ 12 m b.l.f. of fine-grained sediment (Fig. 3). Penetration into sediments and core recovery below 12 m b.l.f. were impossible with the HPC due to the presence of coarser and particularly more consolidated sediments below that depth. The Extended Nose Corer (EXN) was tested in 5073_1_C but resulted in a damaged EXN drill bit and unsatisfactory core recovery. The Alien Coring Tool (ALN) was found to be the only coring tool suitable to advance, with the highest possible core recovery at sediment depths below 12 m b.l.f. (5073_1_C to 5073_1_G, Table 1, Fig. 3). ALN core recovery was high in fine-grained lithologies and even recovered some sand beds throughout the stratigraphy. However, despite the occurrence of the thick coarse-grained strata and the use of rotary coring tools, core recovery and core quality were excellent in fine-grained lithologies. While complete recovery of the coarse-grained deposits was not possible, the project succeeded in the retrieval of representative core sections from these lithologies. A Non-Coring Assembly (NCA)

Table 1. Summary information about the drilled holes during the NamCore drilling (HPC denotes Hydraulic Piston Corer, EXN denotes Extended Nose Corer, ALN denotes Alien Coring Tool). Sediment core recovery is given, excluding core catchers.

Expedition_ Site_Hole	International Generic Sample Number (IGSN)	Longitude (° N) [WGS 84]	Latitude (° E) [WGS84]	Drilled length (m)	Max. cored depth* (m)	Total cored length* (m)	Core recovery (m)	Core recovery (%)	Drill tool	Downhole Logging
5073_1_A	ICDP5073EHG0001	90.690444	30.746639	11.02	10.22	10.93	10.03	91.4	HPC	No
5073_1_B	ICDP5073EHH0001	90.691028	30.747139	11.68	11.68	10.32	10.42	100.5	HPC	No
5073_1_C	ICDP5073EHI0001	90.691083	30.747139	38.91	37.43	42.00	25.82	61.3	EXN, ALN	No
5073_1_D	ICDP5073EHJ0001	90.691139	30.747139	193.83	193.83	168.40	131.53	77.6	ALN	Yes
5073_1_E	ICDP5073EHK0001	90.691220	30.747070	285.95	285.95	282.00	238.43	83.8	ALN	No
5073_1_F	ICDP5073EHL0001	90.691280	30.747020	363.86	363.86	183.00	152.43	82.4	ALN	Yes
5073_1_G	ICDP5073EHM0001	90.691380	30.747090	510.20	510.20	479.34	386.69	79.9	ALN	No
Total				1415.45		1175.99	950.77	80.8		

* Note that the driller's depth for the sediment–water interface was sometimes slightly negative, which can cause an offset between maximum cored depth and total cored length.

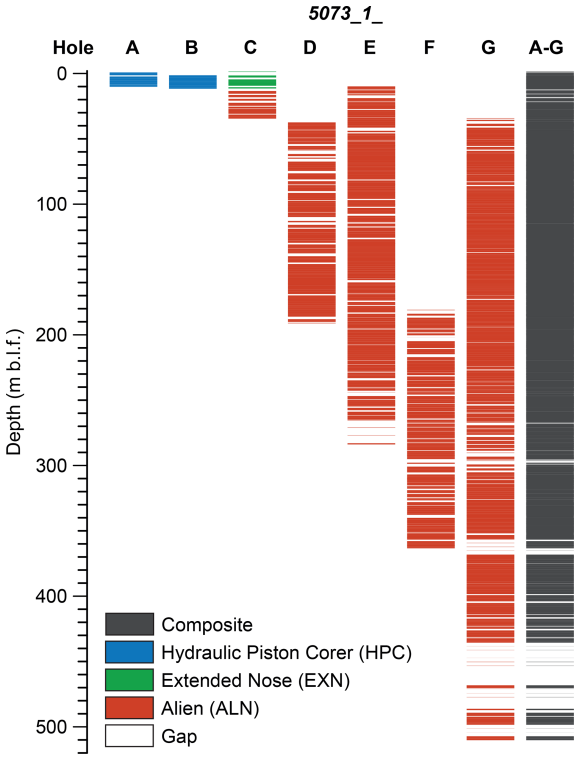

Figure 3. Sediment cores from the NamCore drilling site. Colours indicate coring tools. White parts are either (i) not recovered due to unsuitable lithologies (mostly sand), (ii) core catchers, (iii) noble gas samples, or (iv) reamed using a non-coring assembly (NCA).

was used to drill without core recovery to reach start depths of interest, generally near the depth where coring concluded in a previous hole.

All sediment cores were recovered in standard plastic liners with a 66 mm inner diameter and 3 m length. The bottom face of the sediment core was examined for lithology, and depths were recorded. The drilling fluid was drained from the core liners by gently tipping the cores, and the cores were split into two to four sections (maximum core section length $\leq$ 1.5 m) based on the total length of the recovered sediments, gas cracks, and sections cut for noble gas sampling. Material for microbial and sediment biogeochemistry, such as sedimentary ancient DNA (sedaDNA) and methane concentration, was sampled at core section cuts immediately after splitting (for more details, please see Adolph et al., 2025). Sediment core sections were then capped, sealed, measured, and labelled according to the ICDP standard protocols, including orientation arrows. Core catcher material was bagged, labelled, and stored in cool boxes. Cores were kept vertical until transport to the onshore camp during shift changes. Once ashore, labels were verified, and caps were resealed if needed.

Core catcher processing was performed daily in the onshore lab. Smear slides were prepared and examined under natural and polarized light. Munsell Soil Colours were determined using an x-rite CAPSURE RM200 spectrophotometer. Subsamples were collected for further analysis at home laboratories, including sedimentology, geochemistry, mineralogy, micropaleontology, and luminescence dating. For the upper 10 m of the sediment sequence, porewater was extracted at 20 cm intervals using Rhizon samplers through a hole drilled into the liner. Below, porewater was extracted from pristine and cleaned core catcher samples using a hydraulic press. A detailed description of drilling preparations and technical and on-site operations is published in the operational report (Adolph et al., 2025).

Geophysical downhole logging was carried out for 5073_1_D and 5073_1_F (Table 1), covering the upper 363.86 m b.l.f. The measurements included (i) an acoustic borehole imager; (ii) a dipmeter (caliper, deviation, and deviation direction plus the dip of geological strata); (iii) resistivity (near- and far-field); (iv) magnetic susceptibility (Fig. 4); (v) spectrum gamma radiation including U, Th, and K concentration; (vi) seismic velocity; and (vii) salinity and temperature of the borehole fluid.

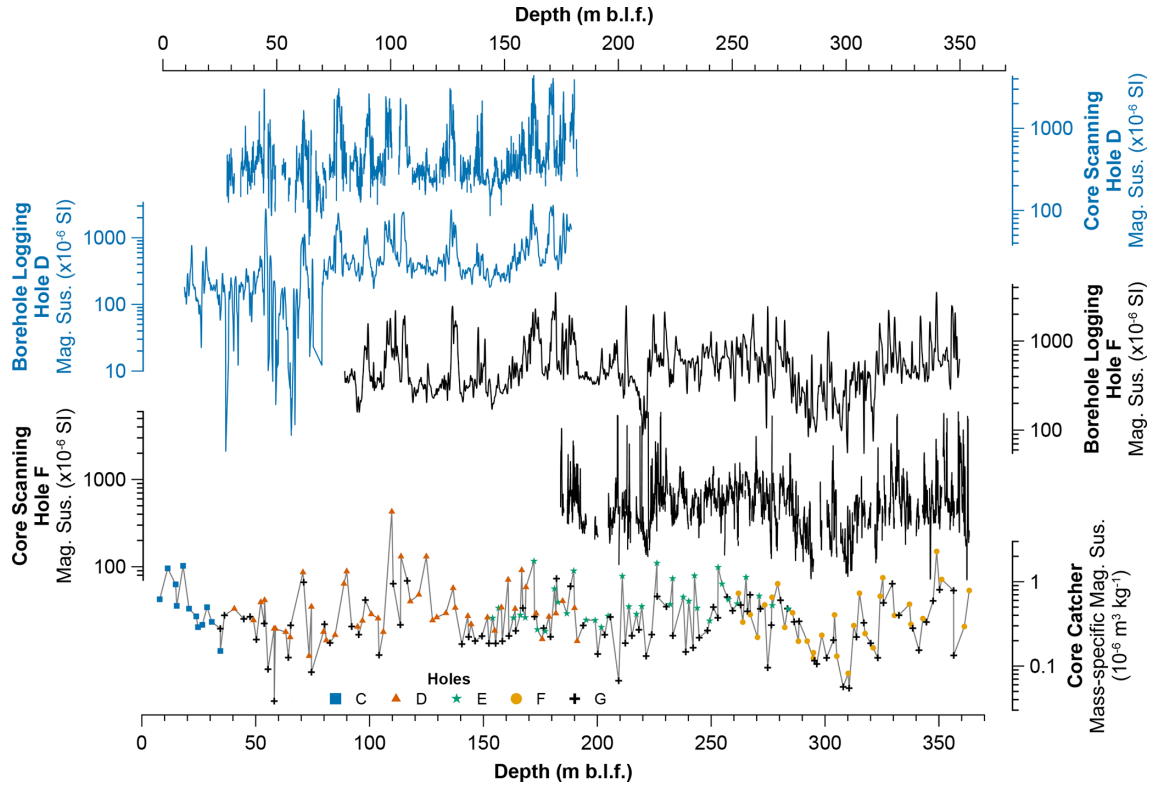

Figure 4. Comparison between magnetic susceptibility data from downhole logging, whole-round measurements, and mass-specific magnetic susceptibility from core catcher material. Downhole logging and whole-round magnetic susceptibility are shown for hole D (blue lines) and hole F (black lines). Mass-specific magnetic susceptibility is a combination of holes C to G, indicated by coloured symbols (C shown by blue square, D shown by orange triangle, E shown by green star, F shown by yellow circle, G shown by black cross). Depths for core data are plotted using the "scaled" depth convention, which fits core recovery > 100 % into the drilled interval using a compression algorithm, equivalent to the IODP CSF-B depth scale, expressed in metres below the lake floor (m b.l.f.).

5 Initial laboratory analysis, sediment core handling, and sediment core description

Before sampling, all drilling-related data were transferred to the ICDP mobile Drilling Information System (mDIS) database, which holds all drilling-related and sampling data and ensures data quality and depth scale control for the whole science team.

5.1 MSCL core scanning and permanent curation

During and after the drilling operations, the sediment core sections were transported to the Institute of Tibetan Plateau Research, Chinese Academy of Sciences, Lhasa, for whole-core multi-sensor logging (MSCL-S, Geotek Ltd.). Measurements included loop sensor magnetic susceptibility and gamma density at 1 cm resolution. Subsequently, sediment core sections were transported to the Institute of Tibetan Plateau Research, Chinese Academy of Sciences, Science City Campus, Beijing, for permanent curation in a repository under refrigerated conditions at +4 °C.

5.2 Core opening, core description, and undrained shear strength

The first core-opening party took place from 8 to 16 February 2025 at the Institute of Tibetan Plateau Research, Chinese Academy of Sciences, Science City Campus, Beijing. Guided by the loop sensor magnetic susceptibility data (Fig. 4), the focus was on opening an overview of the entire stratigraphic sequence using sediment core sections from holes 5073_1_A, 5073_1_B, 5073_1_E, and 5073_1_G. Sediment core sections were split lengthwise into working and archive halves. The archive half was used for undrained shear strength measurements using a handheld penetrometer (Eijkelkamp Inc.) with a measurement interval of < 1 m. The penetrometer was vertically pushed 5 mm into the split core surface. Due to variations in sediment compaction over the entire sediment sequence, we used different tips.

The working half's surface was cleaned for optical imaging using a high-resolution line scan camera (Geoscan-VI camera on an MSCL-S instrument, Geotek Ltd.). The sediment core section description was recorded in PSICAT (v. 1.2.6) and included (i) the lithology; (ii) the predominant

grain size; (iii) the type, thickness, and contact of beddings; (iv) sedimentary textures; and (v) specific sedimentary features (e.g. sand layers, sand lenses, fractures, coring artefacts). Lithological changes were confirmed by smear slide analysis, and carbonate content was tested with HCl. Additionally, samples for ^{14}C dating and µCT analyses were taken.

During the second core-opening and first sampling party from 5 to 18 May 2025, the remaining sediment core sections were split, photographed, and described. Moreover, we established a preliminary splice down to ∼ 250 m based on lithological marker layers and whole-round magnetic susceptibility, which will be refined in the future by XRF scanning results and point sensor magnetic susceptibility. This initial splice was used as the framework for sampling the sediment core sections and for spectrophotometer measurements (Konica Minolta CM-2600d Spectrophotometer). Samples were taken in regular intervals for sedimentology, (micro)-biogeochemistry, micropaleontology, palynology, oxygen, carbon and sulfur isotopes, sedaDNA, and sedimentary pigments. Spectrophotometer measurements were carried out at a 1 cm resolution for the upper 30 m and at a 2 cm resolution below. Additionally, the sediment cores were sampled for dating purposes, e.g. ^{14}C and ^{10}Be dating.

During a second sampling party from 22 to 26 September 2025, we aimed to sample U-channels for core sections down to ∼ 30 m for paleomagnetic analysis and hyperspectral imaging. However, we were only able to extract U-channels to a depth of ∼ 12 m because sediments below were already highly consolidated. Additionally, we took more material for ^{14}C dating. For more details on the core-opening and sampling parties, see the corresponding operational report (Adolph et al., 2025).

5.3 Core catcher analysis

5.3.1 Sedimentology and geochemistry

To obtain an initial overview of sedimentological and geochemical changes, 255 core catcher samples from 5073_1_C to 5073_1_G were analysed in the Physical Geography laboratory of the University of Greifswald, Germany. Visible reflectance spectroscopy (VIS-RS) was applied using a Konica Minolta CM-2600d spectrophotometer (8 mm spot, D65). Basic colorimetric parameters ($L^*a^*b^*$) and reflectance spectra (360–740 nm measurement range in 10 nm steps) were exported from the SpectraMagic NX software (Konica Minolta). The first derivative reflectance spectra were used to determine the initial sediment mineralogical composition, particularly at 555 nm, which may be indicative of hematite (e.g. Balsam et al., 2007).

To determine grain size variations, subsamples from the spectrophotometer analysis were taken and decalcified with hydrochloric acid (4 mL HCl (10 %)). In addition, the organic material was removed by applying hydrogen peroxide (1 mL H_2O_2 (10 %), 2 mL H_2O_2 (35 %)) to the aliquots that were also heated to 70 °C in a water bath. Residues were placed overnight in an overhead shaker. Subsequently, samples were measured using a laser diffraction particle size analyser (Fritsch Analysette 22) in several runs until a reproducible signal was obtained. The first reproducible run was used to calculate grain size statistics using GRADISTAT (v. 9.1; Blott and Pye, 2001). Magnetic susceptibility was measured on freeze-dried, coarsely crushed sediments at both low (0.46 kHz) and high (4.6 kHz) frequencies using a Bartington MS2B sensor following the protocols of Dearing (1999). Mass-specific magnetic susceptibility was calculated by dividing low-frequency measurements by their dry-mass bulk densities. Dry-bulk density was estimated using the dried sample weight and its volume after compressing the sediments in the sample cup. Frequency-dependent magnetic susceptibility is expressed as a percentage.

Carbonate content was determined on ground and homogenized samples by the Scheibler method using 1–2 g of sample material, depending on a pre-test. Loss on ignition (LOI_{550}) was determined on freeze-dried samples by heating the sediment to 550 °C for 3 h in a muffle furnace for holes 5073_1_C to 5073_1_F and the lower part of 5073_1_G.

X-ray fluorescence (XRF) and X-ray diffraction (XRD) analyses were carried out in the Physical Geography laboratory of Friedrich Schiller University, Jena, Germany. Freeze-dried material from 161 core catcher samples was ground in an agate mortar and quantitatively sieved to < 40 µm for homogenization. XRF was performed by using a handheld Bruker S1 TITAN 800-Graphen using the Geo Exploration Calibration set (three phases with 30 s measurement time each). For quality control, standard material by Bruker (CS-M2 800N12862) and a certified standard (LGC 6187 river sediment) were measured. Only elements with values 10 times larger than the error and no values below the limit of detection were considered to be reliable (i.e. Al_2O_3, SiO_2, and K_2O (all calculated as oxides) and Ca, Ti, Fe, Rb, and Sr). XRD was performed using a Bruker D8 Discover equipped with an Eulerian cradle, a single Goebel mirror, and a Vantec 500 area detector at a distance of 28 cm for high 2-Theta resolution. X-rays were produced with a Siemens Copper X-ray source at 40 mV and 40 mA. For data collection, the Bruker GADDS software was used. Data processing, including integration, underground removal, phase identification, and quantification, was performed with the Bruker DiffracEva tool (version 4.1). All diffractograms contained quartz; thus, this mineral was used to enhance accuracy by adjusting the diffractograms to the quartz peaks of the measured range from 6 to 80° 2-Theta.

Altogether, 137 samples were measured for total carbon (TC), total inorganic carbon (TIC), and total nitrogen (TN) at the Institute of Tibetan Plateau Research, Chinese Academy of Sciences, China. TC and TN were measured with a vario MAX cube elemental analyser, and TIC was measured with a Shimadzu TOC (total organic carbon)-VCPH. The TOC was

calculated by subtracting TIC values from TC measurements. The molar TOC / TN ratio was calculated based on molecular weights.

After the core-opening and sampling parties, the core catcher material and results were re-evaluated. The ones contaminated with either drill mud and/or re-cored material (i.e. much softer than the surrounding core material) were excluded from the results.

5.3.2 Micropaleontology

Diatom analysis (∼ 3–18 m sample resolution) was carried out at the Institute of Geosystems and Bioindication, TU Braunschweig, Germany. Samples originated from 5073_1_D, 5073_1_E, 5073_1_F, and 5073_1_G and covered the entire sediment sequence. A total of 84 smear slides were prepared and analysed with a Zeiss Axio Imager.M2 microscope equipped with a Plan-Apochromatic oil immersion objective (× 100/NA1.4) and an AxioCam HRc camera at 1000 × magnification. Selected samples were additionally subjected to a complete diatom preparation (Krahn et al., 2021).

Ostracod analysis was carried out on 43 core catcher samples (∼ 3–35 m sample resolution) at Friedrich Schiller University, Jena, Germany. For each sample, the sediment weight was recorded (10–15 g), and the material was washed through 200 and 63 µm sieves using tap water. The > 200 µm fraction was examined for ostracods and associated microfossils under a low-power stereomicroscope (Zeiss STEMI DV4). Ostracods were semi-quantitatively assessed and assigned to one of four abundance categories based on the estimated number of valves per sample of similar volume: 0, > 10, > 100, and > 1000. The taphonomic state of ostracods was qualitatively evaluated and assigned to one of the following categories, describing the preservation state of the valves: (a) very well preserved, i.e. not abraded translucent shells; (b) well preserved, i.e. with minor traces of abrasion or corrosion and fragmentation; (c) compacted; (d) corroded, i.e. opaque shells with etched surfaces; (e) strongly corroded, i.e. opaque shells with dissolution traces like holes and rounded margins; and (f) stained, with blackish or brownish coatings. Ostracod specimens were documented photographically (Keyence VHX-6000 Digital Microscope) for reference, and taxonomic identifications were carried out using established regional faunal keys from publications (Akita et al., 2015, 2016; Echeverría-Galindo et al., 2021; Peng et al., 2021; Wrozyna et al., 2009).

5.3.3 *n*-alkanes

n-alkane analysis was carried out at the Institute of Tibetan Plateau Research, Chinese Academy of Sciences, China. Altogether, 155 core catcher samples (0.02–20.1 m sample resolution) were analysed. Approximately 8–18 g of lyophilized sediment was extracted, depending on sediment properties and organic matter content, with larger amounts being used for sandy and/or silty samples. Procedural blanks were analysed after every 10 samples, and selected low-response extracts were reanalysed after concentration to confirm compound detectability above background level. Each homogenized and lyophilized sample was ultrasonically extracted four times with a solvent mixture of dichloromethane (DCM) and methanol (MeOH; 9 : 1, v/v). Sulfur was removed from the total lipid extract (TLE) by adding activated copper. All TLEs were saponified and separated into three fractions using silica gel column chromatography and *n*-hexane (apolar hydrocarbons, including *n*-alkanes), DCM (neutral lipids), and MeOH (polar compounds) as respective solvents. The hydrocarbon fractions were re-dissolved in *n*-hexane and subjected to measurement on an Agilent 7890A gas chromatography (GC) equipped with a flame ionization detector (FID) and an Agilent DB-5 column (30 m length × 0.25 mm bore × 0.25 µm film thickness). Compound identification and quantification were achieved by comparison of the retention time and peak area with an external standard (DRH-008S-R2, AccuStandard; 20 ppm, 1 µL injection volume), respectively. P_{aq}, as a proxy for submerged and floating aquatic macrophyte input, was calculated following Ficken et al. (2000). The average chain length (ACL) was calculated according to Poynter and Eglinton (1990). The terrigenous / aquatic ratio of hydrocarbons (TAR_{HC}) was calculated following Bourbonniere and Meyers (1996).

6 Initial coring, core description, core catcher results, and interpretation

6.1 Coring and magnetic susceptibility results

In total, 1415.45 m was drilled and 1175.99 m was cored from seven holes at one site, 5073_1 (Table 1, Fig. 3) while recovering 950.77 m of sediments with an overall core recovery of 80.8 %. The maximum depth reached 510.2 m b.l.f. in 5073_1_G (Table 1). Core recovery was particularly low between 486.2–435.2 m b.l.f., likely due to intercalated, poorly consolidated coarser strata, contrasting in terms of their rheology substantially with the more consolidated fine-grained lithologies. Overall, the sediments are highly consolidated below 321 m b.l.f. Between 321–242 m b.l.f., sediments are recurrently poorly consolidated and coarse-grained, resulting in a higher core loss (Fig. 5). Generally, core recovery was higher in the upper 242 m b.l.f. (Fig. 3) because of predominantly fine-grained sediments (Figs. 3 and 5).

The magnetic susceptibility from (i) downhole logging, (ii) whole-round sediment cores, and (iii) core catcher material shows repeated shifts between lower and higher values. In particular, the downhole logging magnetic susceptibility in the upper ∼ 70 m is low. Generally, we observe widely similar trends across the depth dimension for the upper 356.35 m b.l.f. Given that the downhole logging depth provides an accurate depth scale, the correspondence of the

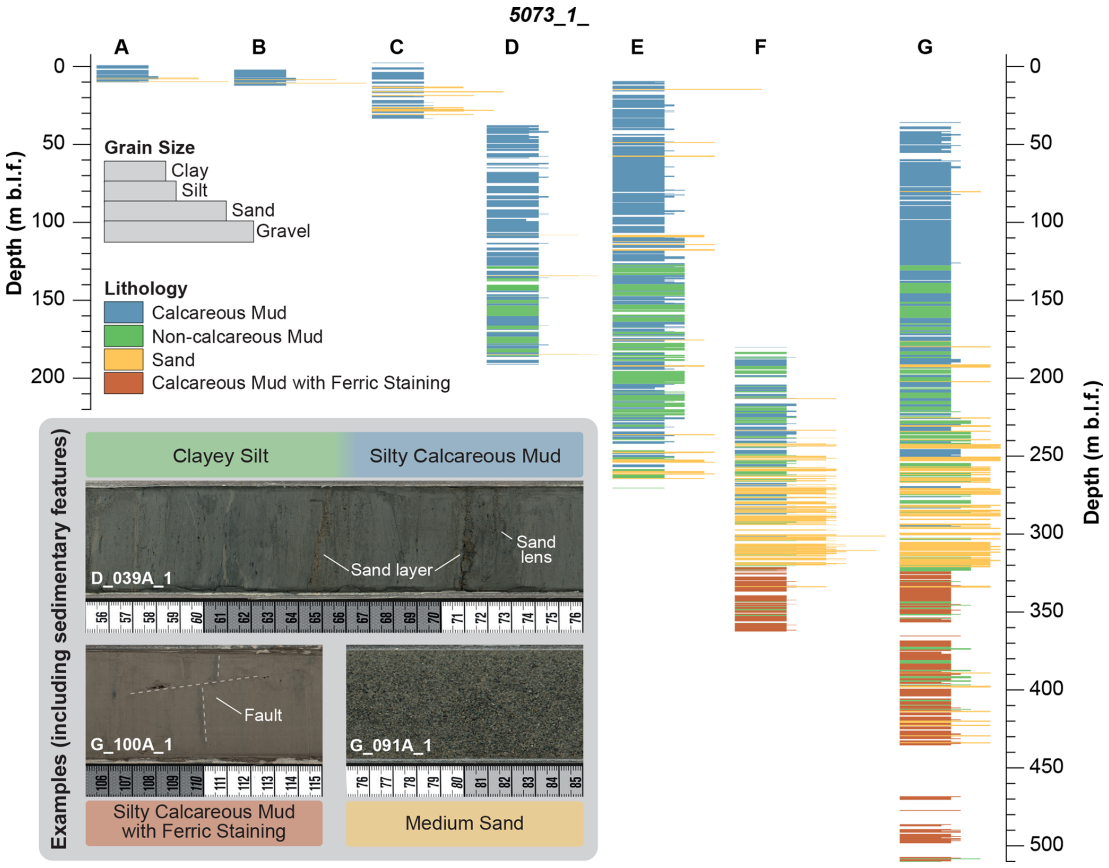

Figure 5. Lithological framework of site 1 across the different boreholes (A–G) based on initial sediment core descriptions. Blank (white) areas indicate sections with no recovery. Four major lithologies were detected, as given in the "Lithology" caption. The inset shows examples of sediment core colour and key sedimentary features (e.g. faults, sand layers and lenses). Note the missing colour change between calcareous and non-calcareous mud.

similar trends in the depth dimension between core and borehole measurements suggests a highly accurate depth control of the drilling depths recorded (Fig. 4).

6.2 Lithological framework

Based on the lithology (Fig. 5) and analyses on core catcher material (Fig. 6a–u), the sediment sequence can be divided into five major lithological units distinguished primarily by shifts in (i) carbonate content, (ii) grain size, (iii) colour, and (iv) frequency-dependent magnetic susceptibility.

Unit 1 (510.12–435.58 m b.l.f.) is characterized by a high core loss and large gaps (Fig. 5), which might have been caused by sediments with sand contents of up to 53 % in the unit's upper part but may also be related to limitations of the drilling equipment and coring tools used for the recovery of these highly consolidated sediments (Fig. 6h). Available sediment core sections are characterized by a shear strength of $> 600\,\mathrm{kN\,m^{-2}}$. The recovered sediment is mostly massive, silty to sandy calcareous mud, intercalated repeatedly by strongly consolidated carbonate layers. Carbonate mineralogy indicates calcite in all samples. Low-magnesium calcite (LMC) and high-Mg calcite (HMC) occur mostly in the lower part (Fig. 6g). Smear slide analysis also suggests aragonite and monohydrocalcite (MHC). Iron-bearing mineral species likely cause subtle ferric staining in unit 1 (a^*, FDS_{555} in Fig. 6a–b). At 487.18 m b.l.f., TIC and carbonate are maximal (8 % and 61 %, Fig. 6d–e), while the frequency-dependent magnetic susceptibility reaches its maximum of 10.9 % (k_{fd}, Fig. 6c). TOC is around 1.4 %, with a TOC / TN of 21 (Fig. 6q–r). In concert, these parameters suggest a terrigenous input (e.g. Dearing et al., 1996; Meyers and Ishiwatari, 1993), which is supported by the presence of organic macro remains, likely of non-aquatic origin and possibly related to a very low lake level.

Unit 2 (435.58–321.15 m b.l.f.) is predominantly composed of silty to sandy calcareous mud with a few non-calcareous mud intervals in between (Fig. 5). The sediment structure varies between massive and finely laminated at the decimetre scale, with fine to medium bedding being the most prevalent structure observed. The calcareous mud intervals have a TIC content of up to 3.5 % (Fig. 6e). Carbonate mineralogy indicates calcite and LMC in almost all

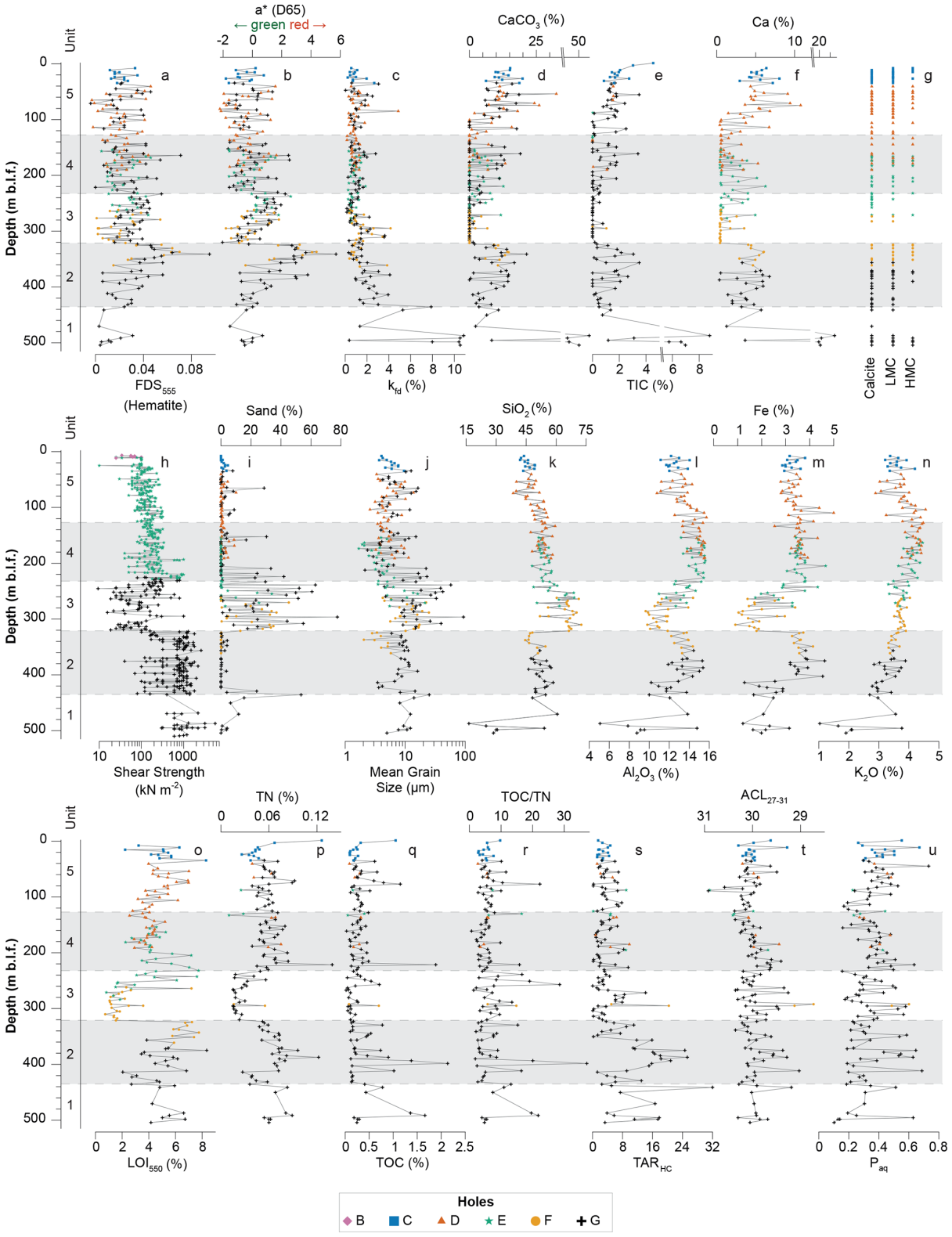

Figure 6. Initial results from the NamCore core catchers. Samples from the individual holes are marked by different symbols in different colours. The sediment sequence is divided into five major sedimentological units (1 to 5). Chemical elements are only shown for elements > 1 %. XRD results were carried out on the same samples as XRF (see Ca) and suggest the varying presence of calcite, low-magnesium calcite (LMC), and high-magnesium calcite (HMC). Please note the axis breaks in $CaCO_3$ and Ca, the logarithmic scale for shear strength and mean grain size, and the inverted axis for $ACL_{27–31}$.

samples, while HMC only occurs above 390.01 m (Fig. 6g). The sediments are repeatedly intercalated by thin sand layers and lenses, as well as pieces of gravel, tentatively identified as dropstones. Such sand layers were not present in the core catchers; consequently, the mean grain size only ranges from 2 to 16 µm (Fig. 6i–j). However, in concert with the frequency-dependent magnetic susceptibility remaining mostly above 2 % below 356.51 m b.l.f. (k_{fd}, Fig. 6c), this may indicate a high terrigenous input, although it is reduced compared to the strata below. Similarly, the TOC has its maximum content of 2.1 % with a TOC / TN of 32 (Fig. 6q–r), suggesting a predominance of terrestrial organic matter at 398.39 m b.l.f. (Meyers and Ishiwatari, 1993). In particular, the topmost part of unit 2 (384.47–324.24 m b.l.f.) has a distinct red hue related to ferric staining (a^*, FDS_{555}, Fig. 6a–b). Shear strength remains high but shows more variability compared to unit 1.

Unit 3 (321.15–242.07 m b.l.f.) predominantly consists of very fine to medium sand, interspersed with calcareous and non-calcareous mud intervals (Fig. 5). Calcareous mud intervals comprise predominantly calcite as the main carbonate phase (Fig. 6g). Frequency-dependent magnetic susceptibility is up to 4.2 % from 321.15 to 265.97 m b.l.f. (Fig. 6c), suggesting an increased terrigenous input. Above, a few layers comprise somewhat elevated organic matter content (TOC, LOI_{550}, TN in Fig. 6o–q) and suggest a predominant terrestrial organic matter source (TOC / TN > 20, Fig. 6r; Meyers and Ishiwatari, 1993). The sand content is up to 77 % (Fig. 6i), which suggests a significant shift in the environmental conditions, possibly to generally lower lake levels and/or increased glacier melt and/or increased fluvial input. These partly opposite interpretations need to be refined based on a more complete dataset in the future. Due to the high sand content, the sediments have a low shear strength (Fig. 6h). However, the mass of these massive and extensive sand layers likely contributed to the strong consolidation of the sediments below.

Unit 4 (242.07–127.66 m b.l.f.) is characterized by recurrent shifts between calcareous and non-calcareous mud (Fig. 5), also reflected in TIC, $CaCO_3$, and Ca contents (Fig. 6d–f). These shifts are not recognizable in colour and/or lightness variations (Fig. 5), i.e. unlike other lacustrine settings, where such optical variation is typical (e.g. Adolph et al., 2024, 2023; Debret et al., 2011). Carbonate mineralogy suggests an abundance of calcite, LMC, and HMC recurrently (Fig. 6g). Compared to the calcareous mud intervals in unit 2, ferric staining is rarely observed (a^* mostly < 0, Fig. 6b). TOC is generally < 0.5 % in all but one instance at 221.44 m b.l.f. (1.9 % TOC, Fig. 6q). Grain size is highly variable between the core catcher samples in this unit. Coarser grain sizes prevail in 5073_1_G to 209.39 m b.l.f. compared to in 5073_1_E, where sand only prevails to 253.05 m b.l.f. (Fig. 6i–j). Shear strength gradually decreases, and frequency-dependent magnetic susceptibility is constantly low (< 2 %, Fig. 6c, h). In concert with a generally decreased sand content, this suggests an overall decreased terrigenous input compared to units below.

Unit 5 (127.66–0 m b.l.f.) is composed of predominantly silty to sandy calcareous mud (Fig. 5), which is massive to finely laminated and partly interspersed with sand layers, sand lenses, and sometimes pieces of gravel (assumed to be dropstones). The carbonate content gradually increases to values of up to 4.5 % TIC at the top of the sediment record (Fig. 6e). Carbonate mineralogy shows an abundance of calcite, LMC, and HMC, with varying concentrations at different depths (Fig. 6g). Organic matter content is often < 0.5 % TOC but has excursions too, e.g. 1.1 % at 77.01 m b.l.f. (Fig. 6q). Grain size is mostly < 10 µm in 5073_1_D, while 5073_1_G shows excursions to coarser grain sizes and an increased sand content (Fig. 6i–j).

Even though the distance between most holes is predominantly < 12 m (Fig. 1), we repeatedly observed (i) differences in thickness between similar lithologies, (ii) varying manifestations of lithological features (e.g. sand layers and lenses), and (iii) variations in grain sizes between the holes. In particular, 5073_1_G generally exhibits coarser grain sizes and thicker sand layers throughout the entire record compared to the other holes (Fig. 5). This observation is supported by the overall trends in the mean grain size and sand percentage, where 5073_1_G is generally at the higher end of the grain size range compared to other holes (Fig. 6i–j). The difference is less pronounced in unit 3 due to the generally coarser-grained sediments, but it is particularly visible in unit 2. This may suggest that 5073_1_G might have been, for example, located closer to a primary source of clastic input and/or in an area with a stronger current activity and/or a steeper slope section prone to sediment gravity flows, which all might have allowed for the deposition of coarser clastic material. The cause of this offset and its consequence for interpreting the sediment record needs to be further explored, but such major deviations have not been observed in other parameters (Fig. 6).

6.3 *n*-alkanes

n-alkanes have been widely applied in paleoenvironmental research (e.g. Kou et al., 2024; Mügler et al., 2008; Strobel et al., 2022; Strobel et al., 2024). Lacustrine sediments often contain a mixed signal of *n*-alkanes from aquatic and terrestrial sources, which can be distinguished by their *n*-alkane chain length (e.g. Ficken et al., 2000; Strobel et al., 2021). Traditionally, long-chain *n*-alkanes (i.e. $n\text{–}C_{27}\text{–}C_{31}$) are thought to be produced by higher terrestrial plants, while short- and mid-chain *n*-alkanes (i.e. $n\text{–}C_{15}\text{–}C_{25}$) are produced by algae and aquatic macrophytes (e.g. Sachse et al., 2012). However, this *n*-alkane source attribution is not always trivial because some aquatic plants can also synthesize larger quantities of longer-chain *n*-alkanes (e.g. Strobel et al., 2021).

The P_{aq} ratio differentiates between the relative contribution of submerged and/or floating aquatic macrophyte input (n–C_{23}, n–C_{25}) against terrestrial plant input (n–C_{29}, n–C_{31}) to lake sediments (Ficken et al., 2000) and has been used to reconstruct the paleohydrological evolution of lakes and peats (e.g. Günther et al., 2016; He et al., 2014; Seki et al., 2009). Here, the P_{aq} ranges from 0.10 to 0.73, with an average of 0.36 (Fig. 6u). In the lower part of the sequence (equivalent to unit 5, 510.12–435.58 m b.l.f.), P_{aq} remains relatively low (average of 0.28), with minor short-term fluctuations. Between 435.58–321.15 m b.l.f., values show a slight increasing trend to values up to 0.35 and moderate variability. From 321.15 to 242.07 m b.l.f., P_{aq} exhibits several short-lived excursions up to 0.60, followed by a gradual decline from 242.07 to 116.20 m b.l.f., where the values decrease from about 0.5 to 0.2. Above 116.20 m b.l.f., P_{aq} shows a gradual increasing trend toward the top of the core. Some studies have demonstrated that environmental factors, including temperature, light availability, salinity, and nutrient conditions, may affect the P_{aq} ratio (Deegan et al., 2005; Rooney and Kalff, 2000). Therefore, its environmental significance should be evaluated with respect to lake basin morphology (Rooney and Kalff, 2000). Based on modern n-alkane distributions in large and deep lakes on the Tibetan Plateau (Kou et al., 2020; Wang et al., 2012), the P_{aq} could be influenced by a combination of water temperature and lake-level variations, with the influence of temperature being more pronounced during periods of high-lake-level stands.

The $ACL_{27–35}$ index is usually used to characterize the chain length distribution of long-chain n-alkanes (Poynter and Eglinton, 1990). Here, the $ACL_{27–35}$ shows comparatively minor fluctuations, mostly ranging from 28.7 to 30.9, with an average chain length of 30.0 (Fig. 6t). In the lower part of the record (510.12–435.58 m b.l.f.), values range from 29.5 to 30.0, with only slight variations. A slight decrease to $\sim$29.5 is observed between 435.58 and 321.15 m b.l.f., followed by an increase and enhanced oscillations from 321.15 to 242.07 m b.l.f. The upper part of the sequence (242.07–0 m b.l.f.) shows relatively stable $ACL_{27–35}$ values ($\sim$29.8–30.2), indicating limited variation in long-chain n-alkane distributions and a persistent vegetation pattern. Eley and Hren (2018) suggested that the ACL is related to the mean annual vapour pressure deficit (VPD), indicating its potential as a proxy for atmospheric moisture conditions. This can be attributed to the main function of plant epicuticular wax, which is to maintain the leaf's water balance. During phases of enhanced evaporation, i.e. drier climatic conditions, long-chain n-alkanes are preferentially synthesized to reduce cuticular water loss associated with evaporation (Riederer and Markstaedter, 1996). Therefore, the $ACL_{27–35}$ is negatively correlated with atmospheric moisture; i.e. a longer n-alkane chain length could indicate drier climatic conditions, which could also translate into glacial–interglacial cycles (Fig. 6; Eley and Hren, 2018; Kou et al., 2024) but needs to be validated in future investigations.

The TAR represents the relative contribution of terrestrial versus aquatic n-alkanes (Bourbonniere and Meyers, 1996). In the lower part of the sequence (510.12–242.07 m b.l.f.), the TAR exhibits the most pronounced variability and several sharp peaks, with the highest values exceeding 30, indicating strong contributions of terrestrial n-alkane input, which correlates to an increased terrigenous input suggested by sedimentological parameters (Fig. 6s). Three major episodes of oscillatory rises occur at 510.12–435.58, 413.79–350.30, and 320.06–242.07 m b.l.f. Toward the top (242.07–0 m b.l.f.), the TAR remains relatively low and stable, generally below 10, with a few minor fluctuations. High TAR values may result either from lake shrinkage, which shortens the transport distance from the shoreline to the lake centre, or from enhanced run-off caused by more intense rainfalls (Meyers and Ishiwatari, 1993), the nature of which will require more detailed investigation of the NamCore sediment record.

6.4 Diatoms

We found very few diatom valves, mostly single fragments, in 12 of the 84 investigated core catcher samples. Even after complete diatom preparation (Krahn et al., 2021) and intensive examination, no additional diatom valve fragments were found. Due to the almost complete absence of diatom valves in the samples examined, in-depth diatom analyses based on established morphological identification using valves have been challenging. However, paleogenetic methods (sedaDNA) could compensate for that issue, particularly because it has already been demonstrated that such methods can be successfully applied at other sites in Nam Co (e.g. Anslan et al., 2020, 2022; Kang et al., 2021).

6.5 Ostracods

Ostracods are the only fossils recovered from the $>200\,\mu m$ fraction of the selected core catcher samples; no molluscs or chironomids were identified. Their abundance and species composition vary strongly between samples (Fig. 7a), ranging from complete absence to more than 1000 valves per $\sim$10 g sediment. Approximately half of the samples contain more than 100 valves (Fig. 7a). In total, six ostracod taxa were identified: *Leucocytherella sinensis* (Huang, 1982), ?*Leucocythere dorsotuberosa* (Huang, 1982), ?*Leucocythere postilirata* (Pang, 1985), *Ilyocypris* ?*bradyi* (Sars, 1890), juvenile *Candona*, and *Ilyocypris* sp. (smooth). No more than five species occur in any single sample, possibly suggesting an overall low ostracod diversity.

Preservation of ostracod valves is highly variable both between and within samples (Fig. 7), ranging from well-preserved, translucent, and non-fragmented valves to strongly fragmented or compacted material. The co-occurrence of multiple preservation states within individual samples likely reflects time-averaging related to the large sampling increments. In addition, the wide sample spacing

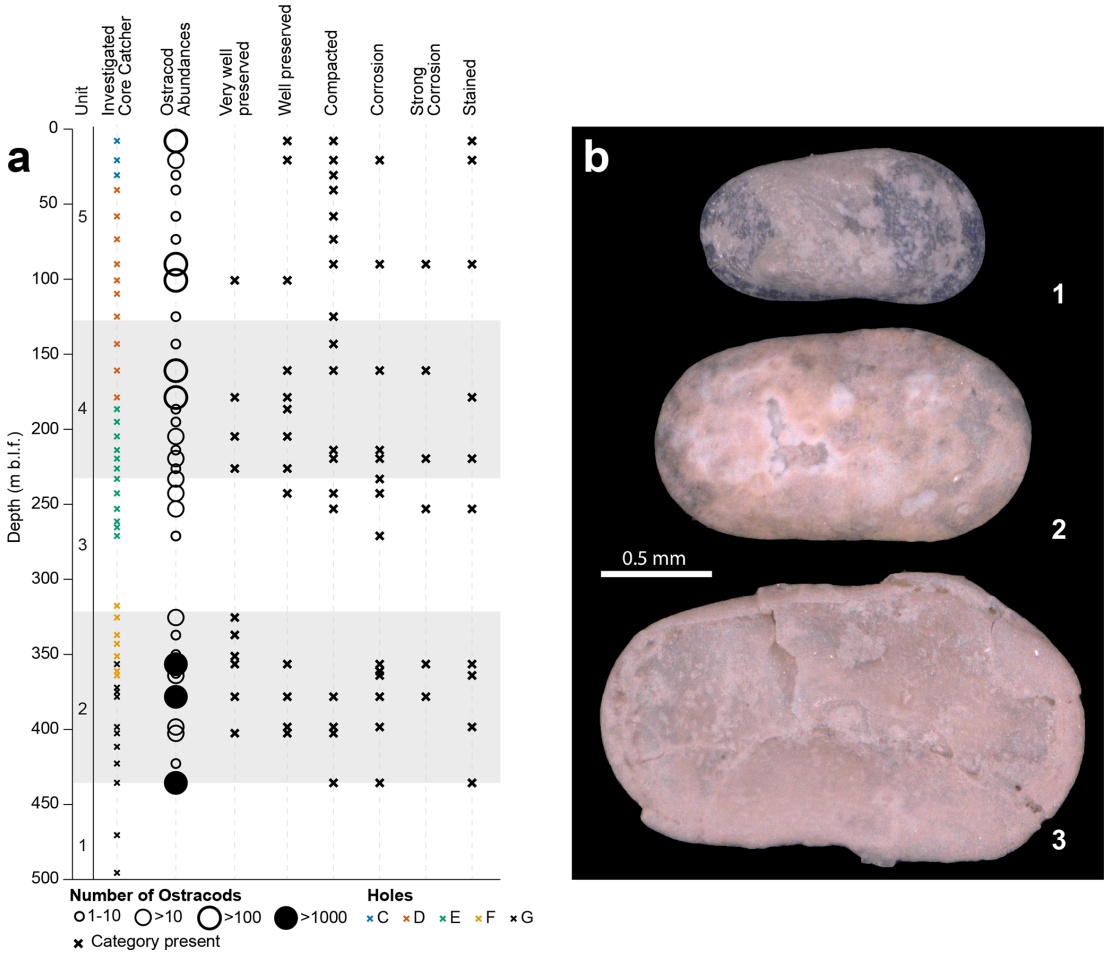

Figure 7. **(a)** Distribution of ostracod abundances and taphonomic features (very well preserved, well preserved, compacted, etc.) along the core depth. Symbol sizes in the ostracod column show semi-quantitative abundance classes. Qualitative taphonomic categories identified in each sample are indicated by "x": from a few to many. No samples were analysed from ~ 270 to 320 m b.l.f. **(b)** Examples for different states of preservation of ostracod shells from core catcher samples. 1 – ?*Leucocythere dorsotuberosa*, well preserved (5073_1_E_067A_3); 2 – *Ilyocypris* sp. with traces of etching (5073_1_E_083A_4); 3 – *Ilyocypris* sp., deformed by compaction (5073_1_E_070A_3).

currently precludes the identification of robust preservation or abundance patterns that could be confidently linked to environmental changes; this issue will be addressed in future analyses.

Below 470.43 m b.l.f., ostracods are absent (Fig. 7), which may indicate unfavourable ecological conditions or post-depositional loss of valves during sediment diagenesis (Akita, 2016; Curry and Filippelli, 2010). In contrast, the sample at 435.58 m b.l.f. contains exceptionally high ostracod abundances (> 1000 valves), dominated by *Leucocytherella sinensis* with subordinate ?*Leucocythere* and *Ilyocypris* sp. Many of these valves are fragmented or coated, which is consistent with the high sand content observed in the uppermost sample of unit 5.

From 422.71 to 219.54 m b.l.f., the ostracod assemblage is dominated by *Ilyocypris* sp., ?*Leucocythere* sp., and juvenile candonids. Abundances and preservation states fluctuate throughout this interval, likely reflecting variable environmental conditions (Fig. 7). Between 213.86 and 7.85 m b.l.f., the dominant taxa shift to *L. sinensis* and ?*L. dorsotuberosa*, representing an ostracod fauna broadly comparable to the modern assemblage (Wrozyna et al., 2009). Although relative abundances of taxa continue to vary within this upper section, preservation is generally good. Two intervals, 143.16–109.76 and 73.43–30.72 m b.l.f., are characterized by a very poor ostracod record. In combination with the predominantly fine-grained and partly non-calcareous sediments observed in these intervals (Figs. 5–6), this pattern may indicate sedimentation under profundal lake conditions.

7 Conclusions and scientific outlook

While our in-depth analyses of the recovered sediments are just at the beginning, the initial results from lithological sed-

iment core descriptions and various analyses on core catcher material suggest that the NamCore sedimentary record reflects the evolution of a highly dynamic high-altitude lake system. Sediments from 510.20–435.58 m b.l.f. may represent an early lake stage and/or a very-low-lake-level phase. Coarse-grained sediments from 321.15–242.07 m b.l.f. exemplify distinctly different sedimentation processes likely related to pronounced environmental changes. Diatoms are mostly absent from the core catcher samples, which could be related to unsuitable growing conditions and/or preservation conditions.

The next analytical steps will include a wide range of geochronological, sedimentological, geochemical, geophysical, and biological approaches, for which samples have already been taken during the sampling parties. The chronology will be assembled by a combination of ^{14}C dating, ^{10}Be dating, magnetostratigraphy, luminescence dating, and amino acid racemization. Granulometric, inorganic, and organic geochemical and geophysical methods are being applied to understand the (hydro)climate history of the Tibetan Plateau and its influence on the (micro-)biological processes, evolution, and resilience of high-altitude ecosystems during both glacial and interglacial climate conditions. Biomarkers, palynology, and ostracods will reveal the dynamics of the evolving terrestrial and aquatic biota on the Tibetan Plateau. Analyses of sediment methane concentrations and their isotopic signature (C, H), sulfur isotopes, and the composition of microbial communities in the sediments will reveal the deep biosphere diversity and activity in these (mostly) carbonate-rich sediments. Early diagenetic processes and ideal diagenetic mineral targets will be identified to study environmental, microbial, and fluid-emanation-related factors contributing to post-depositional alteration of sediment composition. Additionally, to better understand redox processes, the biogeochemical cycles of redox-sensitive elements (e.g. N, Fe, S) in Nam Co's sediments will be explored under controlled conditions using sediment laboratory analogues, i.e. microfluidic experiments. This experimental approach enables non-invasive spatiotemporal monitoring of microbially mediated redox processes at the micro-scale in confined environments, mimicking the heterogeneous structure of sediments and, if properly engineered, their chemical composition (e.g. Ceriotti et al., 2022). Moreover, the water column structure and composition, as well as pore water samples, will be analysed to assess recent and past environmental conditions, as well as the physical and ecological state of Nam Co.

Data availability. The data will be available at https://dataservices.gfz-potsdam.de/panmetaworks/review/3cf967b (last access: 3 June 2026).

Author contributions. Conceptualization: MLA, JW, LZ, LC, AH, HV, GD, VS, DA, NB, JV, TH. Data curation: MLA, JW, LZ, GD, JJ, QK, OS, AS, AU, CZh, BG, MH, CK, AL, ML, QM, PM, KM, XZ. Funding acquisition: JW, LZ, LC, AH, HV, GD, VS, DA, NB, RK, JV, CW, CZe, TH. Investigation: MLA, JW, LZ, LC, AH, HV, GD, PF, JJ, QK, DM, OS, AS, VS, AU, CZh, EB, GC, BG, MH, RK, WK, CK, AL, ML, QM, PM, KM, RO, SO, MP, AP, CT, MV, CW, CZe, XZ, TH. Project Administration: MLA, JW, LZ, LC, AH, HV, JJ, AN, TH. Visualization: MLA, PF, QK, OS, VS. Writing (original draft): MLA, LZ, HV, GD, PF, QK, OS, MH, AN. Writing (review and editing): MLA, JW, LZ, LC, AH, HV, GD, PF, OS, TB, GC, MH, CK, AN, MP, CT, JV, CW, CZe, TH. Software: MLA, BG, MH, CK.

Competing interests. The contact author has declared that none of the authors has any competing interests.

Disclaimer. Publisher's note: Copernicus Publications remains neutral with regard to jurisdictional claims made in the text, published maps, institutional affiliations, or any other geographical representation in this paper. The authors bear the ultimate responsibility for providing appropriate place names. Views expressed in the text are those of the authors and do not necessarily reflect the views of the publisher.

Acknowledgements. The US Continental Scientific Drilling Facility (CSD), Sichuan Huafeng Drilling, Dragon Machinery, the LIAG Institute for Applied Geophysics, the Institute for Tibetan Plateau Research of the Chinese Academy of Sciences (ITPCAS), and the ICDP Operational Support Group are acknowledged for their logistical assistance to the project. This research was carried out with permission from the Tibetan Autonomous Region government. We would like to thank Pierre Francus for the constructive comments on the paper.

Financial support. The Nam Co Drilling Project (ICDP NamCore) was supported by the International Continental Scientific Drilling Program. The ICDP NamCore project received financial support from the Swiss National Science Foundation (SNSF) through a Sinergia grant (no. CRSII5_213522) awarded to H. Vogel. The project was additionally supported by the Natural Environment Research Council (UKRI NERC) (grant no. NE/W000989/1) and received funding from the China MOST Project (grant no. 2019QZKK0202), the National Natural Science Foundation of China (NSFC project no. 42330514), and the Institute of Tibetan Plateau Research, Chinese Academy of Sciences (ITP-CAS) Self-deployment Project (grant no. E0Ty031001). Moreover, it was funded by the Deutsche Forschungsgemeinschaft (DFG, German Research Foundation) – grant nos. 537667198 and 5364373.

Review statement. This paper was edited by Nadine Hallmann and reviewed by Pierre Francus and one anonymous referee.

References

Adolph, M.-L., Dressler, M., Troelstra, V., Wrozyna, C., and Haberzettl, T.: Eutrophication and contamination dynamics of Schweriner See, NE-Germany, during the past 670 years – A multi-proxy approach on lacustrine surface sediments and sediment cores, Sci. Total Environ., 877, 162745, https://doi.org/10.1016/j.scitotenv.2023.162745, 2023.

Adolph, M.-L., Czerwiński, S., Dressler, M., Strobel, P., Bliedtner, M., Lorenz, S., Debret, M., and Haberzettl, T.: North Atlantic Oscillation polarity during the past 3000 years derived from sediments of a large lowland lake, Schweriner See, in NE Germany, Clim. Past, 20, 2143–2165, https://doi.org/10.5194/cp-20-2143-2024, 2024.

Adolph, M.-L., Wang, J., Zhu, L., Clarke, L. J., Henderson, A. C. G., Vogel, H., Hofmann, P., Ju, J., Kunkel, C., Noren, A., Schnurrenberger, D., Spiess, V., Thomas, C., Ulfers, A., and Haberzettl, T.: The Nam Co Drilling Project, Tibet (NamCore): A one-million-year sedimentary record from the Third Pole: Operational Report, Potsdam, 41 pp., https://doi.org/10.48440/ICDP.5073.001, 2025.

Ai, K., Shi, G., Zhang, K., Ji, J., Song, B., Shen, T., and Guo, S.: The uppermost Oligocene Kailas flora from southern Tibetan Plateau and its implications for the uplift history of the southern Lhasa terrane, Palaeogeogr. Palaeocl., 515, 143–151, https://doi.org/10.1016/j.palaeo.2018.04.017, 2019.

Aitchison, J. C., Ali, J. R., and Davis, A. M.: When and where did India and Asia collide?, J. Geophys. Res.-Sol. Ea., 112, 1–19, https://doi.org/10.1029/2006jb004706, 2007.

Akita, L. G.: Ostracodes as indicators of Late Quaternary aquatic and monsoon system changes on the southern Tibetan Plateau, PhD Thesis, Friedrich Schiller University, Jena, https://www.db-thueringen.de/receive/dbt_mods_00029216 (last access: 3 June 2026), 2016.

Akita, L. G., Frenzel, P., Haberzettl, T., Kasper, T., Wang, J., and Reicherter, K.: Ostracoda (Crustacea) as indicators of subaqueous mass movements: An example from the large brackish lake Tangra Yumco on the southern Tibetan Plateau, China, Palaeogeogr. Palaeocl., 419, 60–74, https://doi.org/10.1016/j.palaeo.2014.08.003, 2015.

Akita, L. G., Frenzel, P., Wang, J., Börner, N., and Peng, P.: Spatial distribution and ecology of the Recent Ostracoda from Tangra Yumco and adjacent waters on the southern Tibetan Plateau: A key to palaeoenvironmental reconstruction, Limnologica, 59, 21–43, https://doi.org/10.1016/j.limno.2016.03.005, 2016.

Anslan, S., Azizi Rad, M., Buckel, J., Echeverria Galindo, P., Kai, J., Kang, W., Keys, L., Maurischat, P., Nieberding, F., Reinosch, E., Tang, H., Tran, T. V., Wang, Y., and Schwalb, A.: Reviews and syntheses: How do abiotic and biotic processes respond to climatic variations in the Nam Co catchment (Tibetan Plateau)?, Biogeosciences, 17, 1261–1279, https://doi.org/10.5194/bg-17-1261-2020, 2020.

Anslan, S., Kang, W. A., Dulias, K., Wuennemann, B., Echeverria-Galindo, P., Börner, N., Schwarz, A., Liu, Y. Q., Liu, K. S., Kuenzel, S., Kisand, V., Rioual, P., Peng, P., Wang, J. B., Zhu, L. P., Vences, M., and Schwalb, A.: Compatibility of Diatom Valve Records With Sedimentary Ancient DNA Amplicon Data: A Case Study in a Brackish, Alkaline Tibetan Lake, Front. Earth Sci., 10, 1–14, https://doi.org/10.3389/feart.2022.824656, 2022.

Ariztegui, D., Thomas, C., and Vuillemin, A.: Present and future of subsurface biosphere studies in lacustrine sediments through scientific drilling, Int. J. Earth Sci., 104, 1655–1665, https://doi.org/10.1007/s00531-015-1148-4, 2015.

Armijo, R., Tapponnier, P., Mercier, J. L., and Han, T.-L.: Quaternary extension in southern Tibet: Field observations and tectonic implications, J. Geophys. Res.-Sol. Ea., 91, 13803–13872, https://doi.org/10.1029/JB091iB14p13803, 1986.

Armijo, R., Tapponnier, P., and Han, T.: Late Cenozoic right-lateral strike-slip faulting in southern Tibet, J. Geophys. Res.-Sol. Ea., 94, 2787–2838, https://doi.org/10.1029/JB094iB03p02787, 1989.

Balsam, W., Damuth, J. E., and Deaton, B.: Marine sediment components: identification and dispersal assessed by diffuse reflectance spectrophotometry, International Journal of Environment and Health, 1, 403–426, https://doi.org/10.1504/ijenvh.2007.017869, 2007.

Blott, S. J. and Pye, K.: GRADISTAT: A grain size distribution and statistics package for the analysis of unconsolidated sediments, Earth Surf. Proc. Land., 26, 1237–1248, https://doi.org/10.1002/esp.261, 2001.

Bourbonniere, R. A. and Meyers, P. A.: Anthropogenic influences on hydrocarbon contents of sediments deposited in eastern Lake Ontario since 1800, Environ. Geol., 28, 22–28, https://doi.org/10.1007/s002540050074, 1996.

Ceriotti, G., Borisov, S. M., Berg, J. S., and de Anna, P.: Morphology and Size of Bacterial Colonies Control Anoxic Microenvironment Formation in Porous Media, Environ. Sci. Technol., 56, 17471–17480, https://doi.org/10.1021/acs.est.2c05842, 2022.

Chen, J., Zhang, Q., Huang, W., Lu, Z., Zhang, Z., and Chen, F.: Northwestward shift of the northern boundary of the East Asian summer monsoon during the mid-Holocene caused by orbital forcing and vegetation feedbacks, Quaternary Sci. Rev., 268, https://doi.org/10.1016/j.quascirev.2021.107136, 2021.

Chevalier, M. L., Tapponnier, P., van der Woerd, J., Leloup, P. H., Wang, S., Pan, J., Bai, M., Kali, E., Liu, X., and Li, H.: Late Quaternary Extension Rates Across the Northern Half of the Yadong-Gulu Rift: Implication for East-West Extension in Southern Tibet, J. Geophys. Res.-Sol. Ea., 125, https://doi.org/10.1029/2019jb019106, 2020.

Clemens, S. C., Kuhnt, W., LeVay, L. J., and the Expedition 353 Scientists, 2016: Indian Monsoon Rainfall, Proceedings of the International Ocean Discovery Program, 353: College Station, TX (International Ocean Discovery Program), https://doi.org/10.14379/iodp.proc.353.2016, 2016.

Curry, B. B. and Filippelli, G. M.: Episodes of low dissolved oxygen indicated by ostracodes and sediment geochemistry at Crystal Lake, Illinois, USA, Limnol. Oceanogr., 55, 2403–2423, https://doi.org/10.4319/lo.2010.55.6.2403, 2010.

Daut, G., Mäusbacher, R., Baade, J., Gleixner, G., Kroemer, E., Mügler, I., Wallner, J., Wang, J., and Zhu, L.: Late Quaternary hydrological changes inferred from lake level fluctuations of Nam Co (Tibetan Plateau, China), Quatern. Int., 218, 86–93, https://doi.org/10.1016/j.quaint.2010.01.001, 2010.

Dearing, J. A.: Environmental Magnetic Susceptibility. Using the Bartington MS2 System, 43 pp., ISBN 0952340909, 1999.

Dearing, J. A., Dann, R. J. L., Hay, K., Lees, J. A., Loveland, P. J., Maher, B. A., and OGrady, K.: Frequency-dependent susceptibility measurements of environmental materials, Geo-

phys. J. Int., 124, 228–240, https://doi.org/10.1111/j.1365-246X.1996.tb06366.x, 1996.

Debret, M., Sebag, D., Desmet, M., Balsam, W., Copard, Y., Mourier, B., Susperrigui, A. S., Arnaud, F., Bentaleb, I., Chapron, E., Lallier-Vergès, E., and Winiarski, T.: Spectrocolorimetric interpretation of sedimentary dynamics: The new "Q7/4 diagram", Earth-Sci. Rev., 109, 1–19, https://doi.org/10.1016/j.earscirev.2011.07.002, 2011.

Deegan, B., Harrington, T. J., and Dundon, P.: Effects of salinity and inundation regime on growth and distribution of Schoenoplectus triqueter, Aquat. Bot., 81, 199–211, https://doi.org/10.1016/j.aquabot.2004.11.006, 2005.

Dietze, E., Maussion, F., Ahlborn, M., Diekmann, B., Hartmann, K., Henkel, K., Kasper, T., Lockot, G., Opitz, S., and Haberzettl, T.: Sediment transport processes across the Tibetan Plateau inferred from robust grain-size end members in lake sediments, Clim. Past, 10, 91–106, https://doi.org/10.5194/cp-10-91-2014, 2014.

Ding, L., Xu, Q., Yue, Y., Wang, H., Cai, F., and Li, S.: The Andean-type Gangdese Mountains: Paleoelevation record from the Paleocene–Eocene Linzhou Basin, Earth Planet. Sc. Lett., 392, 250–264, https://doi.org/10.1016/j.epsl.2014.01.045, 2014.

Ding, L., Kapp, P., Cai, F., Garzione, C. N., Xiong, Z., Wang, H., and Wang, C.: Timing and mechanisms of Tibetan Plateau uplift, Nat. Rev. Earth. Environ., 3, 652–667, https://doi.org/10.1038/s43017-022-00318-4, 2022.

Doberschütz, S., Frenzel, P., Haberzettl, T., Kasper, T., Wang, J., Zhu, L., Daut, G., Schwalb, A., and Mäusbacher, R.: Monsoonal forcing of Holocene paleoenvironmental change on the central Tibetan Plateau inferred using a sediment record from Lake Nam Co (Xizang, China), J. Paleolimnol., 51, 253–266, https://doi.org/10.1007/s10933-013-9702-1, 2013.

Echeverría-Galindo, P., Anslan, S., Frenzel, P., Künzel, S., Vences, M., Pérez, L., Börner, N., Kang, W., Schwarz, A., Wang, J., Peng, P., Zhu, L., and Schwalb, A.: High-throughput identification of non-marine Ostracoda from the Tibetan Plateau: Evaluating the success of various primers on sedimentary DNA samples, Environmental DNA, 3, 982–996, https://doi.org/10.1002/edn3.222, 2021.

Eley, Y. L. and Hren, M. T.: Reconstructing vapor pressure deficit from leaf wax lipid molecular distributions, Sci. Rep., 8, 3967, https://doi.org/10.1038/s41598-018-21959-w, 2018.

Ficken, K. J., Li, B., Swain, D. L., and Eglinton, G.: An *n*-alkane proxy for the sedimentary input of submerged/floating freshwater aquatic macrophytes, Org. Geochem., 31, 745–749, https://doi.org/10.1016/S0146-6380(00)00081-4, 2000.

Gibbons, A. D., Zahirovic, S., Müller, R. D., Whittaker, J. M., and Yatheesh, V.: A tectonic model reconciling evidence for the collisions between India, Eurasia and intra-oceanic arcs of the central-eastern Tethys, Gondwana Res., 28, 451–492, https://doi.org/10.1016/j.gr.2015.01.001, 2015.

Günther, F., Thiele, A., Biskop, S., Mäusbacher, R., Haberzettl, T., Yao, T., and Gleixner, G.: Late quaternary hydrological changes at Tangra Yumco, Tibetan Plateau: a compound-specific isotope-based quantification of lake level changes, J. Paleolimnol., 55, 369–382, https://doi.org/10.1007/s10933-016-9887-1, 2016.

Guo, B., Nie, J., Stevens, T., Buylaert, J.-P., Peng, T., Xiao, W., Pan, B., and Fang, X.: Dominant precessional forcing of the East Asian summer monsoon since 260 ka, Geology, 50, 1372–1376, https://doi.org/10.1130/g50206.1, 2022.

Haberzettl, T., Daut, G., Schulze, N., Spiess, V., Wang, J., Zhu, L., and the 2018 Nam Co workshop party: ICDP workshop on scientific drilling of Nam Co on the Tibetan Plateau: 1 million years of paleoenvironmental history, geomicrobiology, tectonics and paleomagnetism derived from sediments of a high-altitude lake, Sci. Dril., 25, 63–70, https://doi.org/10.5194/sd-25-63-2019, 2019.

He, Y., Zheng, Y., Pan, A., Zhao, C., Sun, Y., Song, M., Zheng, Z., and Liu, Z.: Biomarker-based reconstructions of Holocene lake-level changes at Lake Gahai on the northeastern Tibetan Plateau, Holocene, 24, 405–412, https://doi.org/10.1177/0959683613519689, 2014.

Henderson, A. C. G., Wang, J., Zhu, L. P., Haberzettl, T., Ju, J., Vogel, H., and Clarke, L.: The Nam Co Drilling Project, Tibet Plateau (NamCore): A one-million-year sedimentary record from the Third Pole, Past Global Changes Magazine, 32, 76–77, https://doi.org/10.22498/pages.32.2.76, 2024.

Kang, W., Anslan, S., Börner, N., Schwarz, A., Schmidt, R., Künzel, S., Rioual, P., Echeverría-Galindo, P., Vences, M., Wang, J., and Schwalb, A.: Diatom metabarcoding and microscopic analyses from sediment samples at Lake Nam Co, Tibet: The effect of sample-size and bioinformatics on the identified communities, Ecol. Indic., 121, https://doi.org/10.1016/j.ecolind.2020.107070, 2021.

Kapp, J. L. D. A., Harrison, T. M., Kapp, P., Grove, M., Lovera, O. M., and Lin, D.: Nyainqentanglha Shan: A window into the tectonic, thermal, and geochemical evolution of the Lhasa block, southern Tibet, J. Geophys. Res.-Sol. Ea., 110, https://doi.org/10.1029/2004jb003330, 2005.

Kasper, T., Haberzettl, T., Doberschütz, S., Daut, G., Wang, J., Zhu, L., Nowaczyk, N., and Mäusbacher, R.: Indian Ocean Summer Monsoon (IOSM)-dynamics within the past 4 ka recorded in the sediments of Lake Nam Co, central Tibetan Plateau (China), Quaternary Sci. Rev., 39, 7-3-85, https://doi.org/10.1016/j.quascirev.2012.02.011, 2012.

Kasper, T., Haberzettl, T., Wang, J. B., Daut, G., Doberschütz, S., Zhu, L. P., and Mäusbacher, R.: Hydrological variations on the Central Tibetan Plateau since the Last Glacial Maximum and their teleconnection to inter-regional and hemispheric climate variations, J. Quaternary Sci., 30, 70–78, https://doi.org/10.1002/jqs.2759, 2015.

Kasper, T., Wang, J., Schwalb, A., Daut, G., Plessen, B., Zhu, L., Mäusbacher, R., and Haberzettl, T.: Precipitation dynamics on the Tibetan Plateau during the Late Quaternary – Hydroclimatic sedimentary proxies versus lake level variability, Global Planet. Change, 205, https://doi.org/10.1016/j.gloplacha.2021.103594, 2021.

Kou, Q., Lin, X., Wang, J., Yu, S., Kai, J., Laug, A., and Zhu, L.: Spatial distribution of n-alkanes in surface sediments of Selin Co Lake, central Tibetan Plateau, China, J. Paleolimnol., 65, 53–67, https://doi.org/10.1007/s10933-020-00148-8, 2020.

Kou, Q., Zhu, L., Wang, J., Ma, Q., and Ju, J.: Reconstruction of temperature and hydroclimate in Serling Co (Central Tibet) since the last deglaciation, Palaeogeogr. Palaeocl., 655, https://doi.org/10.1016/j.palaeo.2024.112557, 2024.

Krahn, K. J., Schwarz, A., Wetzel, C. E., Cohuo-Durán, S., Daut, G., Macario-González, L., Pérez, L., Wang, J., and Schwalb,

A.: Three new needle-shaped *Fragilaria* species from Central America and the Tibetan Plateau, Phytotaxa, 479, 1–22, https://doi.org/10.11646/phytotaxa.479.1.1, 2021.

Li, K., Tapponnier, P., Xu, X., Ren, J., Wang, S., and Zhao, J.: Holocene Slip Rate Along the Beng Co Fault and Dextral Strike-Slip Extrusion of Central Eastern Tibet, Tectonics, 41, https://doi.org/10.1029/2022tc007230, 2022.

Maussion, F., Scherer, D., Mölg, T., Collier, E., Curio, J., and Finkelnburg, R.: Precipitation Seasonality and Variability over the Tibetan Plateau as Resolved by the High Asia Reanalysis, J. Climate, 27, 1910–1927, https://doi.org/10.1175/jcli-d-13-00282.1, 2014.

Meyers, P. A. and Ishiwatari, R.: Lacustrine Organic Geochemistry – an Overview of Indicators of Organic-Matter Sources and Diagenesis in Lake-Sediments, Org. Geochem., 20, 867–900, https://doi.org/10.1016/0146-6380(93)90100-P, 1993.

Mosbrugger, V., Favre, A., Muellner-Riehl, A. N., Päckert, M., and Mulch, A.: Cenozoic evolution of geobiodiversity in the Tibeto-Himalayan region, in: Mountains, climate and biodiversity, edited by: Hoorn, C., Perrigo, A., and Antonelli, A., John Wiley & Sons Ltd, 429–448, ISBN 9781119159896, 2018.

Mügler, I., Sachse, D., Werner, M., Xu, B., Wu, G., Yao, T., and Gleixner, G.: Effect of lake evaporation on δD values of lacustrine n-alkanes: A comparison of Nam Co (Tibetan Plateau) and Holzmaar (Germany), Org. Geochem., 39, 711–729, https://doi.org/10.1016/j.orggeochem.2008.02.008, 2008.

Peng, P., Zhai, D., Smith, R. J., Wang, Q., Guo, Y., and Zhu, L.: On some modern Ostracoda (Crustacea) from the Tibetan Plateau in SW China, with descriptions of three new species, Zootaxa, 4942, 501–542, https://doi.org/10.11646/zootaxa.4942.4.2, 2021.

Poynter, J. G. and Eglinton, G.: Molecular composition of three sediments from Hole 717C: The Bengal Fan, Proceedings of the Ocean Drilling Program, Scientific Results, 116, https://www-odp.tamu.edu/publications/116_SR/VOLUME/CHAPTERS/sr116_14.pdf (last access: 3 June 2026), 1990.

Pullen, A., Kapp, P., Gehrels, G. E., DeCelles, P. G., Brown, E. H., Fabijanic, J. M., and Ding, L.: Gangdese retroarc thrust belt and foreland basin deposits in the Damxung area, southern Tibet, J. Asian Earth Sci., 33, 323–336, https://doi.org/10.1016/j.jseaes.2008.01.005, 2008.

Riederer, M. and Markstaedter, C.: Cuticular waxes – a critical assessment of current knowledge, in: Plant Cuticles – an integrated functional approach, edited by: Kerstiens, G., BIOS Scientific Publishers, Oxford, ISBN 1859961304, 1996.

Rooney, N. and Kalff, J.: Inter-annual variation in submerged macrophyte community biomass and distribution: the influence of temperature and lake morphometry, Aquat. Bot., 68, 321–335, https://doi.org/10.1016/S0304-3770(00)00126-1, 2000.

Sachse, D., Billault, I., Bowen, G. J., Chikaraishi, Y., Dawson, T. E., Feakins, S. J., Freeman, K. H., Magill, C. R., McInerney, F. A., van der Meer, M. T. J., Polissar, P., Robins, R. J., Sachs, J. P., Schmidt, H. L., Sessions, A. L., White, J. W. C., West, J. B., and Kahmen, A.: Molecular Paleohydrology: Interpreting the Hydrogen-Isotopic Composition of Lipid Biomarkers from Photosynthesizing Organisms, Annu. Rev. Earth Pl. Sc., 40, 221–249, https://doi.org/10.1146/annurev-earth-042711-105535, 2012.

Schulze, N.: The Sedimentary and Tectonic Evolution of the Nam Co Basin, Tibetan Plateau, since the Middle Pleistocene – A Seismoacoustic Study on Lake Sediments, Geosciences, PhD Thesis, University of Bremen, Bremen, 154 pp., https://doi.org/10.26092/elib/567, 2020.

Seki, O., Meyers, P. A., Kawamura, K., Zheng, Y., and Zhou, W.: Hydrogen isotopic ratios of plant wax n-alkanes in a peat bog deposited in northeast China during the last 16 kyr, Org. Geochem., 40, 671–677, https://doi.org/10.1016/j.orggeochem.2009.03.007, 2009.

Stevens, T., Buylaert, J. P., Thiel, C., Ujvari, G., Yi, S., Murray, A. S., Frechen, M., and Lu, H.: Ice-volume-forced erosion of the Chinese Loess Plateau global Quaternary stratotype site, Nat. Commun., 9, 983, https://doi.org/10.1038/s41467-018-03329-2, 2018.

Strobel, P., Struck, J., Zech, R., and Bliedtner, M.: The spatial distribution of sedimentary compounds and their environmental implications in surface sediments of Lake Khar Nuur (Mongolian Altai), Earth Surf. Proc. Land., 46, 611–625, https://doi.org/10.1002/esp.5049, 2021.

Strobel, P., Bliedtner, M., Carr, A. S., Struck, J., du Plessis, N., Glaser, B., Meadows, M. E., Quick, L. J., Zech, M., Zech, R., and Haberzettl, T.: Reconstructing Late Quaternary precipitation and its source on the southern Cape coast of South Africa: A multi-proxy paleoenvironmental record from Vankervelsvlei, Quaternary Sci. Rev., 284, https://doi.org/10.1016/j.quascirev.2022.107467, 2022.

Strobel, P., Henning, T., Bliedtner, M., Mosher, S. G., Rahimova, H., Haberzettl, T., Kirsten, K. L., Lehndorff, E., Power, M. J., Zech, M., and Zech, R.: Holocene fire dynamics and their climatic controls on the southern Cape coast of South Africa – A 7.2 ka multi-proxy record from the peatland Vankervelsvlei, Quaternary Sci. Rev., 325, https://doi.org/10.1016/j.quascirev.2023.108464, 2024.

Taylor, M. and Yin, A.: Active structures of the Himalayan-Tibetan orogen and their relationships to earthquake distribution, contemporary strain field, and Cenozoic volcanism, Geosphere, 5, 199–214, https://doi.org/10.1130/ges00217.1, 2009.

Thomas, C., Wang, J., Berg, J., Haberzettl, T., Kipfer, R., Vogel, H., DIGESTED Science Team, and NamCore Drilling Team: Living in the deep at the top of the world, Past Global Changes Magazine, 32, 124–125, https://doi.org/10.22498/pages.32.2.124, 2024.

United Nations Environment Programme: A Scientific Assessment of the Third Pole Environment, Nairobi, 52, , https://wedocs.unep.org/handle/20.500.11822/39757 (last access: 3 June 2026), 2022.

von Oheimb, P. V., Albrecht, C., Riedel, F., Du, L., Yang, J., Aldridge, D. C., Bossneck, U., Zhang, H., and Wilke, T.: Freshwater biogeography and limnological evolution of the Tibetan Plateau – insights from a plateau-wide distributed gastropod taxon (Radix spp.), PLoS One, 6, 1–9, https://doi.org/10.1371/journal.pone.0026307, 2011.

Wang, J., Zhu, L., Daut, G., Ju, J., Lin, X., Wang, Y., and Zhen, X.: Investigation of bathymetry and water quality of Lake Nam Co, the largest lake on the central Tibetan Plateau, China, Limnology, 10, 149–158, https://doi.org/10.1007/s10201-009-0266-8, 2009.

Wang, J., Huang, L., Ju, J., Daut, G., Wang, Y., Ma, Q., Zhu, L., Haberzettl, T., Baade, J., and Mäusbacher, R.:

Spatial and temporal variations in water temperature in a high-altitude deep dimictic mountain lake (Nam Co), central Tibetan Plateau, J. Great Lakes Res., 45, 212–223, https://doi.org/10.1016/j.jglr.2018.12.005, 2019.

Wang, J., Huang, L., Ju, J., Daut, G., Ma, Q., Zhu, L., Haberzettl, T., Baade, J., Mäusbacher, R., Hamilton, A., Graves, K., Olsthoorn, J., and Laval, B. E.: Seasonal stratification of a deep, high-altitude, dimictic lake: Nam Co, Tibetan Plateau, J. Hydrol., 584, https://doi.org/10.1016/j.jhydrol.2020.124668, 2020.

Wang, J., Wang, L., Li, M., Zhu, L., and Li, X.: Lake volume variation in the endorheic basin of the Tibetan Plateau from 1989 to 2019, Sci. Data, 9, 611, https://doi.org/10.1038/s41597-022-01711-w, 2022.

Wang, Y., Zhu, L., Wang, J., Ju, J., and Lin, X.: The spatial distribution and sedimentary processes of organic matter in surface sediments of Nam Co, Central Tibetan Plateau, Chinese Sci. Bull., 57, 4753–4764, https://doi.org/10.1007/s11434-012-5500-9, 2012.

Wrozyna, C., Frenzel, P., Xie, M., Zhu, L., and Schwalb, A.: A taxonomical and ecological overview of Recent and Holocene ostracodes of the Nam Co region, southern Tibet, Quaternary Sciences, 29, 665–677, 2009.

Wrozyna, C., Frenzel, P., Daut, G., Mäusbacher, R., Zhu, L., and Schwalb, A.: Chapter 16 – Holocene Lake-Level Changes of Lake Nam Co, Tibetan Plateau, Deduced from Ostracod Assemblages and $\delta^{18}O$ and $\delta^{13}C$ Signatures of Their Valves, in: Ostracoda as Proxies for Quaternary Climate Change, edited by: David, J. H., Jonathan, A. H., Julio, R.-L., and Finn, A. V., Developments in Quaternary Sciences, Elsevier, 281–295, https://doi.org/10.1016/B978-0-444-53636-5.00016-0, 2012.

Wu, Z., Ye, P., Barosh, P. J., and Wu, Z.: The October 6, 2008 Mw 6.3 magnitude Damxung earthquake, Yadong-Gulu rift, Tibet, and implications for present-day crustal deformation within Tibet, J. Asian Earth Sci., 40, 943–957, https://doi.org/10.1016/j.jseaes.2010.05.003, 2011.

Xu, Q., Ding, L., Spicer, R. A., Liu, X., Li, S., and Wang, H.: Stable isotopes reveal southward growth of the Himalayan-Tibetan Plateau since the Paleocene, Gondwana Res., 54, 50–61, https://doi.org/10.1016/j.gr.2017.10.005, 2018.

Yao, T., Masson-Delmotte, V., Gao, J., Yu, W., Yang, X., Risi, C., Sturm, C., Werner, M., Zhao, H., He, Y., Ren, W., Tian, L., Shi, C., and Hou, S.: A review of climatic controls on $\delta^{18}O$ in precipitation over the Tibetan Plateau: Observations and simulations, Rev. Geophys., 51, 525–548, https://doi.org/10.1002/rog.20023, 2013.

Yao, T., Bolch, T., Chen, D., Gao, J., Immerzeel, W., Piao, S., Su, F., Thompson, L., Wada, Y., Wang, L., Wang, T., Wu, G., Xu, B., Yang, W., Zhang, G., and Zhao, P.: The imbalance of the Asian water tower, Nat. Rev. Earth. Environ., 3, 618–632, https://doi.org/10.1038/s43017-022-00299-4, 2022.

Zhou, S., Kang, S., Chen, F., and Joswiak, D. R.: Water balance observations reveal significant subsurface water seepage from Lake Nam Co, south-central Tibetan Plateau, J. Hydrol., 491, 89–99, https://doi.org/10.1016/j.jhydrol.2013.03.030, 2013.

Zhu, L., Ju, J., Qiao, B., Liu, C., Wang, J., Yang, R., Ma, Q., Guo, L., and Pang, S.: Physical and biogeochemical responses of Tibetan Plateau lakes to climate change, Nat. Rev. Earth. Environ., 6, 284–298, https://doi.org/10.1038/s43017-025-00650-5, 2025.